[redacted]

CENTRAL RESEARCH LIBRARY
DOCUMENT COLLECTION

AEC RESEARCH AND DEVELOPMENT REPORT

ORNL-2340, Part 6
C-85 – Reactors – Aircraft Nuclear Propulsion Systems

cy. 126A

MARTIN MARIETTA ENERGY SYSTEMS LIBRARIES
3 4456 0251030 7

DECLASSIFIED
CLASSIFICATION CHANGED TO:
BY AUTHORITY OF: AEC 1-25-66
BY: E. Lackenmeister 2-14-67

AIRCRAFT NUCLEAR PROPULSION PROJECT

QUARTERLY PROGRESS REPORT

FOR PERIOD ENDING JUNE 30, 1957

CENTRAL RESEARCH LIBRARY
DOCUMENT COLLECTION
LIBRARY LOAN COPY
DO NOT TRANSFER TO ANOTHER PERSON
If you wish someone else to see this document, send in name with document and the library will arrange a loan.

[redacted]

OAK RIDGE NATIONAL LABORATORY
OPERATED BY
UNION CARBIDE NUCLEAR COMPANY
A Division of Union Carbide and Carbon Corporation
UCC
POST OFFICE BOX X · OAK RIDGE, TENNESSEE

[redacted]

[redacted]

LEGAL NOTICE

This report was prepared as an account of Government sponsored work. Neither the United States, nor the Commission, nor any person acting on behalf of the Commission:

A. Makes any warranty or representation, express or implied, with respect to the accuracy, completeness, or usefulness of the information contained in this report, or that the use of any information, apparatus, method, or process disclosed in this report may not infringe privately owned rights; or

B. Assumes any liabilities with respect to the use of, or for damages resulting from the use of any information, apparatus, method, or process disclosed in this report.

As used in the above, "person acting on behalf of the Commission" includes any employee or contractor of the Commission to the extent that such employee or contractor prepares, handles or distributes, or provides access to, any information pursuant to his employment or contract with the Commission.

[redacted]

ORNL-2340, Part 6
C-85 – Reactors – Aircraft Nuclear Propulsion Systems

This document consists of 38 pages.

Copy 126 of 225 copies. Series A.

Contract No. W-7405-eng-26

AIRCRAFT NUCLEAR PROPULSION PROJECT

QUARTERLY PROGRESS REPORT

For Period Ending June 30, 1957

W. H. Jordan, Director
S. J. Cromer, Co-Director
A. J. Miller, Assistant Director

DATE ISSUED

OCT 11 1957

OAK RIDGE NATIONAL LABORATORY
Operated by
UNION CARBIDE NUCLEAR COMPANY
A Division of Union Carbide and Carbon Corporation
Post Office Box X
Oak Ridge, Tennessee

MARTIN MARIETTA ENERGY SYSTEMS LIBRARIES

3 4456 0251030 7

[redacted]

[redacted]

ORNL-2340, Part 6
C-85 – Reactors – Aircraft Nuclear Propulsion Systems

INTERNAL DISTRIBUTION

1. R. G. Affel
2. C. J. Barton
3. M. Bender
4. D. S. Billington
5. F. F. Blankenship
6. E. P. Blizard
7. C. J. Borkowski
8. W. F. Boudreau
9. G. E. Boyd
10. M. A. Bredig
11. E. J. Breeding
12. W. E. Browning
13. F. R. Bruce
14. A. D. Callihan
15. D. W. Cardwell
16. C. E. Center (K-25)
17. R. A. Charpie
18. R. L. Clark
19. C. E. Clifford
20. J. H. Coobs
21. W. B. Cottrell
22. S. Cromer
23. R. S. Crouse
24. F. L. Culler
25. D. R. Cuneo
26. J. H. DeVan
27. L. M. Doney
28. D. A. Douglas
29. E. R. Dytko
30. W. K. Eister
31. L. B. Emlet (K-25)
32. D. E. Ferguson
33. A. P. Fraas
34. J. H. Frye
35. W. T. Furgerson
36. R. J. Gray
37. A. T. Gresky
38. W. R. Grimes
39. A. G. Grindell
40. E. Guth
41. C. S. Harrill
42. E. E. Hoffman
43. H. W. Hoffman
44. A. Hollaender
45. A. S. Householder
46. J. T. Howe
47. W. H. Jordan
48. G. W. Keilholtz
49. C. P. Keim
50. F. L. Keller
51. M. T. Kelley
52. F. Kertesz
53. J. J. Keyes
54–55. J. A. Lane
56. R. B. Lindauer
57. R. S. Livingston
58. R. N. Lyon
59. H. G. MacPherson
60. R. E. MacPherson
61. F. C. Maienschein
62. W. D. Manly
63. E. R. Mann
64. L. A. Mann
65. W. B. McDonald
66. J. R. McNally
67. F. R. McQuilkin
68. R. V. Meghreblian
69. R. P. Milford
70. A. J. Miller
71. R. E. Moore
72. J. G. Morgan
73. K. Z. Morgan
74. E. J. Murphy
75. J. P. Murray (Y-12)
76. M. L. Nelson
77. G. J. Nessle
78. R. B. Oliver
79. L. G. Overholser
80. P. Patriarca
81. S. K. Penny
82. A. M. Perry
83. D. Phillips
84. J. C. Pigg
85. P. M. Reyling
86. A. E. Richt
87. M. T. Robinson
88. H. W. Savage
89. A. W. Savolainen
90. R. D. Schultheiss
91. D. Scott

[redacted]

[redacted]

92. J. L. Scott
93. E. D. Shipley
94. A. Simon
95. O. Sisman
96. J. Sites
97. M. J. Skinner
98. A. H. Snell
99. C. D. Susano
100. J. A. Swartout
101. E. H. Taylor
102. R. E. Thoma
103. D. B. Trauger
104. D. K. Trubey
105. G. M. Watson
106. A. M. Weinberg
107. J. C. White
108. G. D. Whitman
109. E. P. Wigner (consultant)
110. G. C. Williams
111. J. C. Wilson
112. C. E. Winters
113. W. Zobel
114–116. ORNL – Y-12 Technical Library Document Reference Section
117–123. Laboratory Records Department
124. Laboratory Records, ORNL R.C.
125–127. Central Research Library

EXTERNAL DISTRIBUTION

128. AF Plant Representative, Baltimore
129. AF Plant Representative, Burbank
130. AF Plant Representative, Clifton
131. AF Plant Representative, Long Beach
132–133. AF Plant Representative, Marietta
134–136. AF Plant Representative, Santa Monica
137–138. AF Plant Representative, Seattle
139. AF Plant Representative, Wichita
140. Air Research and Development Command (RDGN)
141. Air Technical Intelligence Center
142. Air University Library
143–145. ANP Project Office, Fort Worth
146. Argonne National Laboratory
147. Armed Forces Special Weapons Project, Sandia
148. Armed Forces Special Weapons Project, Washington
149. Assistant AF Plant Representative, Downey
150. Assistant Secretary of the Air Force, R&D
151–156. Atomic Energy Commission, Washington
157. Bureau of Aeronautics
158. Bureau of Aeronautics General Representative
159. Chicago Operations Office
160. Chicago Patent Group
161. Chief of Naval Research
162. Convair-General Dynamics Corporation
163. Curtiss-Wright Corporation
164–167. General Electric Company (ANPD)
168. Hartford Area Office
169. Headquarters, Air Force Special Weapons Center
170. Idaho Operations Office
171. Rockland Area Office
172. Los Alamos Scientific Laboratory
173. Marquardt Aircraft Company
174. National Advisory Committee for Aeronautics, Cleveland

[redacted]

[redacted]

175. National Advisory Committee for Aeronautics, Washington
176–178. Naval Air Development and Material Center
179. Naval Research Laboratory
180. North American Aviation, Inc. (Missile Development Division)
181. Nuclear Development Corporation of America
182. Office of Chief of Naval Operations (OP-361)
183. Patent Branch, Washington
184. Patterson-Moos
185–188. Pratt & Whitney Aircraft Division (Fox Project)
189. San Francisco Operations Office
190. Sandia Corporation
191. Sandia Corporation, Livermore
192. School of Aviation Medicine
193. USAF Headquarters
194. USAF Project RAND
195. U.S. Naval Radiological Defense Laboratory
196. University of California Radiation Laboratory, Livermore
197–214. Wright Air Development Center (WCOSI-3)
215–224. Technical Information Service Extension, Oak Ridge
225. Division of Research and Development AEC, ORO

[redacted]

[redacted]

FOREWORD

This portion, Part 6. Advanced Power Plant Design and Aircraft Shielding, of the Aircraft Nuclear Propulsion Project Quarterly Progress Report falls in AEC category C-85, Reactors – Aircraft Nuclear Propulsion Systems, and is therefore being issued separately in order not to further limit distribution of the material that falls in AEC category C-84, Reactors – Special Features of Aircraft Reactors, which has been issued as ORNL-2340, Parts 1–5.

[redacted]

[redacted]

CONTENTS

FOREWORD

SUMMARY 1

PART 6. ADVANCED POWER PLANT DESIGN AND AIRCRAFT SHIELDING

6.1. ADVANCED POWER PLANT DESIGN 5

Parametric Studies of Performance of Circulating-Fuel-Reactor-Powered Aircraft 5

6.2. TOWER SHIELDING FACILITY 8

Irradiation of a Pratt & Whitney Aircraft J-57 Engine 8

Measurements Preceding Engine Irradiation (Phase I) 8

Measurements During Irradiation (Phase II) 9

Measurements Following Engine Irradiation (Phase III) 10

Determination of the Power of the Tower Shielding Facility Reactor 13

Experimental Technique 13

Method of Calculation 16

Results and Discussion 16

Auxiliary Methods of Determining Power Linearity 17

Reproducibility of TSF Data 19

Development of the Hornyak Button as a Fast-Neutron Dosimeter 20

6.3. AIRCRAFT SHIELD DESIGN 28

Monte Carlo Calculations of Fluxes and Dose Rates Resulting from Neutrons Multiply Scattered in Air 28

Calculation of Air-Scattered Neutron Dose Rates Around a Cylindrically Symmetric Source 28

[redacted]

[redacted]

ANP PROJECT QUARTERLY PROGRESS REPORT

SUMMARY

6.1. Advanced Power Plant Design

Studies were completed which show the effect of design variables on the size and performance of (1) a circulating-fuel-reactor-powered aircraft with turboprop engines that would be capable of operating at Mach 0.7 at sea level with a 30,000-lb payload, (2) a similarly powered aircraft with turbojet engines that would be capable of flight at Mach 0.85 at sea level with a 30,000-lb payload, and (3) a similarly powered turbojet aircraft that would be capable of supersonic flight at 35,000 ft with a payload of 10,000 lb. An airframe configuration was developed for such an aircraft that would be capable of flight at Mach 1.5.

6.2. Tower Shielding Facility

The investigation of the effects of nuclear radiation on the control and performance of jet engines was continued by exposing, for a second time, a Pratt & Whitney J-57 model jet engine to nuclear radiation emanating from the TSF reactor. The engine operated successfully for 50 hr in a radiation environment identical, within experimental reproducibility, to that of the first test, and no detrimental effects on control and performance were evident. During the first test the engine lubricating oil was changed every 8 hr, whereas during the second test the oil remained in the engine for the entire 50-hr test run. A sample of the engine oil from the second test was used for absorption, decay, and spectrum studies and revealed a specific saturated activity of 2.17×10^5 dpm/ml for P^{32} and 4.54×10^2 dpm/ml for Na^{24}.

Calorimetric experiments to determine the power of the TSF reactor were conducted weekly during March and bimonthly thereafter to collect sufficient data for a statistical analysis of the results. The results, when plotted with previous data taken at six-month intervals, indicated a trend toward increasing power with time. Thermal-neutron flux measurements on the center line of one fuel element during calorimetric experiments disclosed a shift in power distribution that effected an increase in total power for the element.

Sufficient data have been accumulated on the major variables associated with dose measurements at the Tower Shielding Facility (TSF) to predict the probable error connected with the data. An experimental program to determine the combined error in measurements in which three of the most sensitive variables were considered resulted in establishing a maximum probable error of 2.2%. Thus, if three times the probable error were used, 95% of the TSF data would fall within ±6.6% of the mean.

Additional studies have been made of the Hornyak button in an effort to find the crystal size and composition required to duplicate the response of a Hurst-type fast-neutron dosimeter at various neutron energies. Previous data showed responses that were similar for neutron energies above 1 Mev but which were unsatisfactory for lower energies. New crystals were tested in an attempt to make the low-energy response as good as the high-energy response. The majority of the data were obtained with a monoenergetic neutron flux generated by the Van de Graaff generator. A few crystals were also tested in the spectrum field of the TSF reactor.

6.3. Aircraft Shield Design

A previously developed code for a Monte Carlo calculation of the scattering of neutrons in air has been utilized to determine the flux and dose rate at an isotropic detector located a specified distance from a line beam of neutrons of initial energy E_0 leaving a point source at a polar angle θ_0. Calculations were performed for E_0 = 0.55, 1.2, 2, 3, and 5 Mev, θ_0 = 2, 15, 30, 60, 90, 135, and 180 deg, and separation distances of 5, 10, 20, 40, 64, and 100 ft.

An Oracle code has been written with which the results obtained in the Monte Carlo air-scattering calculation discussed above can be utilized to calculate the neutron dose rate around a cylindrically symmetric source.

[redacted]

Part 6

ADVANCED POWER PLANT DESIGN

S. J. Cromer

AIRCRAFT SHIELDING

E. P. Blizard

6.1. ADVANCED POWER PLANT DESIGN

A. P. Fraas

PARAMETRIC STUDIES OF PERFORMANCE OF CIRCULATING-FUEL-REACTOR-POWERED AIRCRAFT

W. T. Furgerson

Studies have been completed which show the effect of design variables on the size and performance of the circulating-fuel-reactor-powered aircraft that would be required to perform three basic missions. The aircraft and missions studied were:

1. a turboprop aircraft that would be capable of operating at Mach 0.7 at sea level with a 30,000-lb payload,
2. a turbojet aircraft that would be capable of operating at Mach 0.85 at sea level with a 30,000-lb payload,
3. a turbojet aircraft that would be capable of supersonic flight at 35,000 ft with a payload of 10,000 lb.

In each case performance was based on all-nuclear flight.

It was considered that interburning with chemical fuel, if used at all, would be for emergency use in the event of failure of some component of the reactor power system. No allowance was made for the weight involved in carrying chemical fuel. The neutron shield could consist of chemical fuel to be burned in an emergency and a limited additional capacity could be obtained at the expense of the payload.

Reactor and shield weights were calculated from the method given in ORNL-1575 (ref 1) for symmetrical ideal shields. It was assumed that any saving in weight which could be effected by shaping the shield would be offset by the additional weight required for shielding-duct penetrations.

For the two subsonic aircraft the radiation dose rate was assumed to be 10 rem/hr at 50 ft, with the crew compartment rate varying from 0.01 to 1.0 rem/hr. The supersonic aircraft dose rates were fixed at 100 rem/hr at 50 ft and 0.1 rem/hr in the crew compartment. Results of the three studies are shown in Figs. 6.1.1, 6.1.2, and 6.1.3.

It is also important, particularly in the case of supersonic aircraft, not only that the powerplant required to produce the necessary thrust be within its calculated weight limitations, but that its dimensions be such that it can fit into an aircraft configuration which is capable of giving the assumed lift-drag ratio at the design Mach number. For the one particular case of a Mach 1.5 airplane, the powerplant components were laid out by using calculated sizes to obtain dimensions of the entire power system. Finally, an airframe configuration

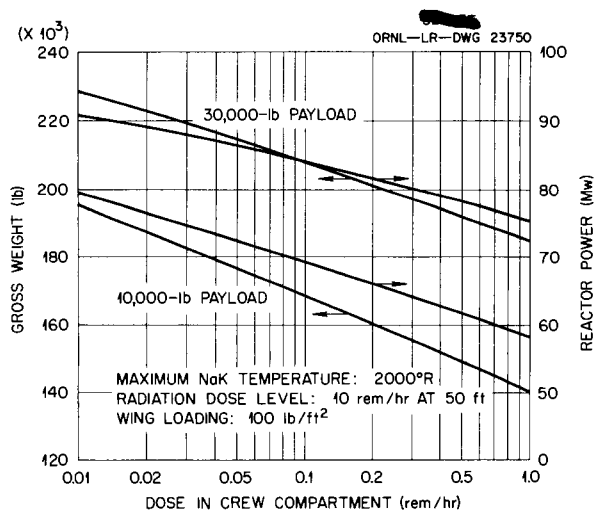

Fig. 6.1.1. Effect of Payload and Dose Rate on Gross Weight and Reactor Power of a Turboprop Aircraft Capable of Operating at Mach 0.7 at Sea Level.

[1] E. P. Blizard and H. Goldstein (eds.), *Report of the 1953 Summer Shielding Session*, ORNL-1575 (July 12, 1954).

with a delta-wing-plan form and a loading of 120 lb/ft^2 was "wrapped" around the power system. Preliminary calculations indicate that the resulting configuration, shown in Fig. 6.1.4, would equal or exceed the assumed lift-drag ratio of 6.

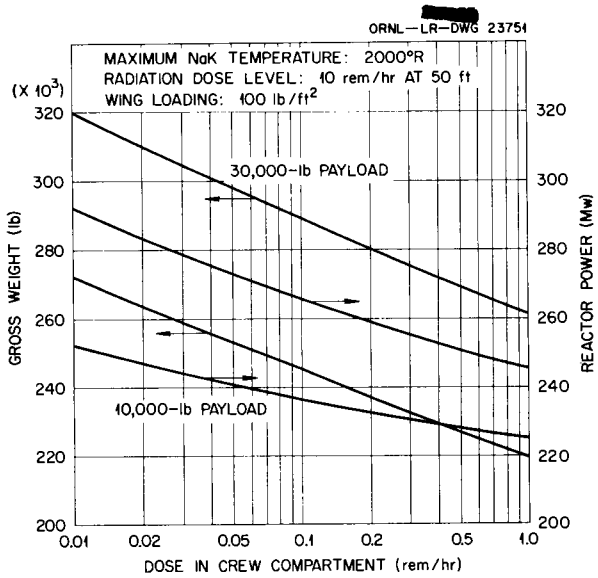

Fig. 6.1.2. Effect of Payload and Dose Rate on Gross Weight and Reactor Power of a Turbojet Aircraft Capable of Operating at Mach 0.85 at Sea Level.

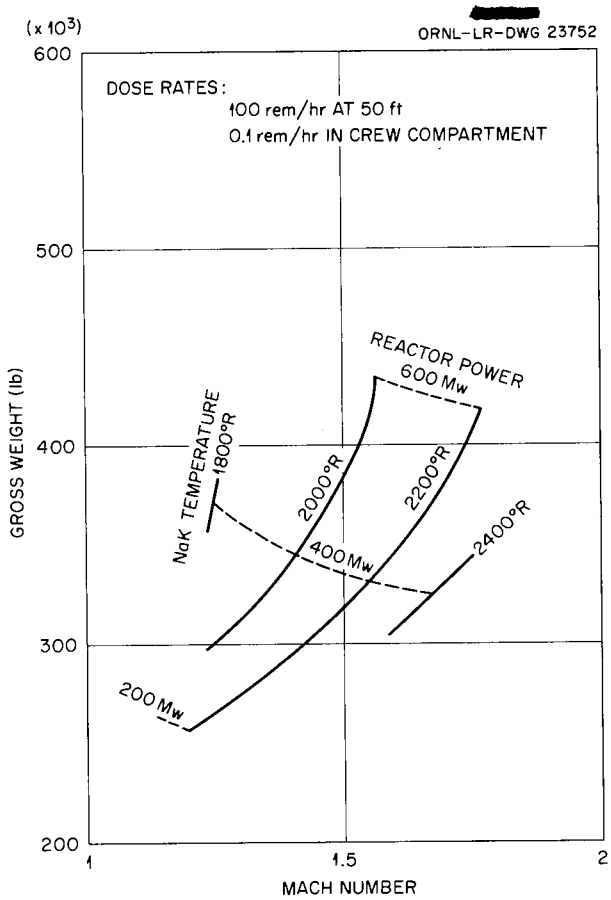

Fig. 6.1.3. Gross Weight in Relation to Mach Number of a Turbojet Aircraft Capable of Supersonic Flight at 35,000 ft with a Payload of 10,000 lb.

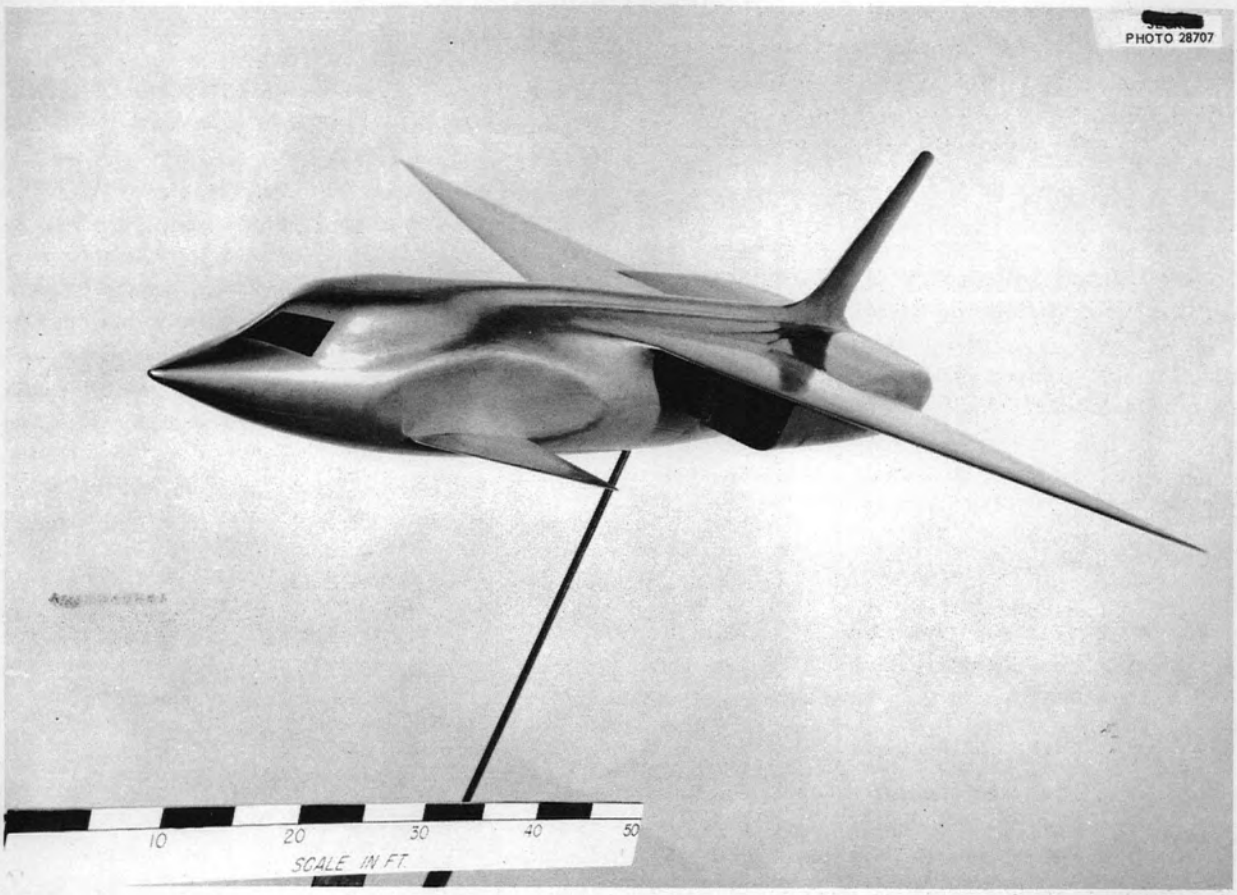

Fig. 6.1.4. Configuration of a Circulating-Fuel-Reactor-Powered Aircraft with Turbojet Engines Capable of Flight at Mach 1.5 at 35,000 ft with a Payload of 10,000 lb.

6.2. TOWER SHIELDING FACILITY

C. E. Clifford

IRRADIATION OF A PRATT & WHITNEY AIRCRAFT J-57 ENGINE

W. J. McCool[1]

The study of the effects of nuclear radiation on the control and performance of jet engines was continued by exposing, for a second time, a Pratt & Whitney J-57 model jet engine to radiation from the TSF reactor. During this second test the engine lubricating oil was not changed at any time, whereas in the first test it was changed every 8 hr. All other experimental conditions were as nearly the same as those for the first test as was possible.

The geometry of the experiment was described previously.[2] The reactor was operated for 50 hr at full power (400-kw nominal power), while the jet engine was operated through various performance cycles periodically to determine the degree of control and to obtain performance data.

As in the first test, the nuclear measurements were divided into three phases. Phase I measurements were made with only the reactor in position; that is, the engine had not yet been placed in position. During the phase I measurements the detectors were located along the line which would coincide with the axis of the engine when it was in place. Phase II measurements were made along the surface of the engine with both the reactor and the engine in position. Some of the phase II measurements extended through the entire 50-hr test period. Phase III measurements included all nuclear measurements made after the termination of the 50-hr test.

Measurements Preceding Engine Irradiation (Phase I)

Since the geometry of the second test was identical to that of the first test, complete traverses of the detector along the line which would coincide with the engine axis were not made during phase I of the experiment. Instead, a spot check of the dose rate was made at the point where the intensities would have a peak value, that is, the intersection between the line coincident with the J-57 axis and the line coincident with the reactor axis. In order to obtain data on which to base corrections for slight differences of water thickness between the reactor and reactor tank wall, measurements of the gamma-ray and neutron dose rates were made at this point of intersection as a function of the reactor water-shield thickness (Figs. 6.2.1 and 6.2.2). In general, the agreement of the data was satisfactory, the disagreement being less than ±10%. The slight divergence of the gamma-ray dose rate curves (Fig. 6.2.2) is

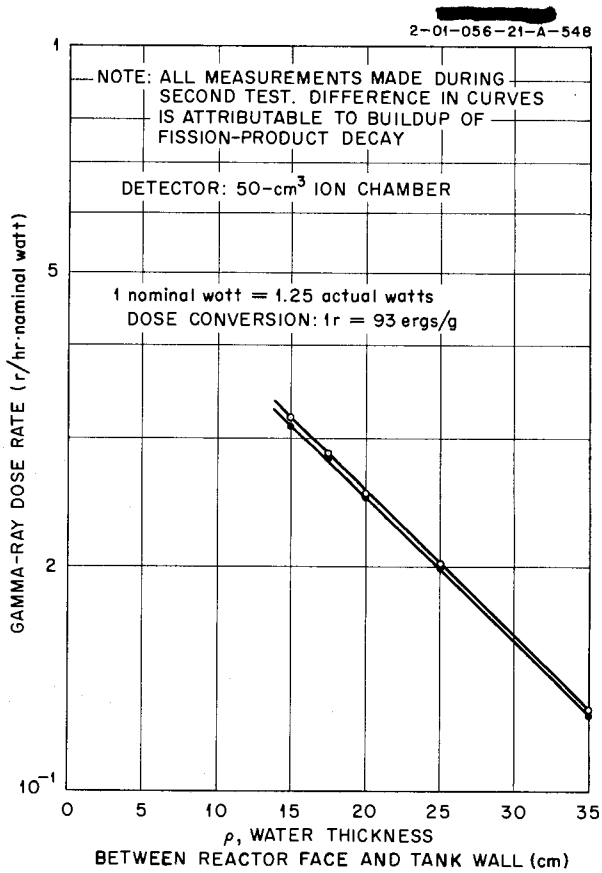

Fig. 6.2.1. Gamma-Ray Dose Rates at the Point of Intersection of a Line Coincident with the J-57 Axis and a Line Coincident with the Reactor Axis as a Function of the Reactor Shield Thickness (Test II, Phase II, Engine Not Present).

[1] On assignment from Pratt & Whitney Aircraft.

[2] W. J. McCool and F. J. Muckenthaler, *ANP Quar. Prog. Rep. Mar. 31, 1957*, ORNL-2274, Part 6, p 11.

caused by the buildup of fission-product decay during the period of about 1 hr that is required to run traverses in both directions.

In a renewed effort to obtain the low-energy neutron flux in which the engine would be placed, "stacked" gold foils were exposed at various positions along the line which would be coincident with the engine axis. Each foil stack consisted of three bare 5-mil-thick gold foils placed one behind the other. The specific disintegration rate of the foils as a function of the distance from the engine tailpipe when it was in position is shown in Fig. 6.2.3.

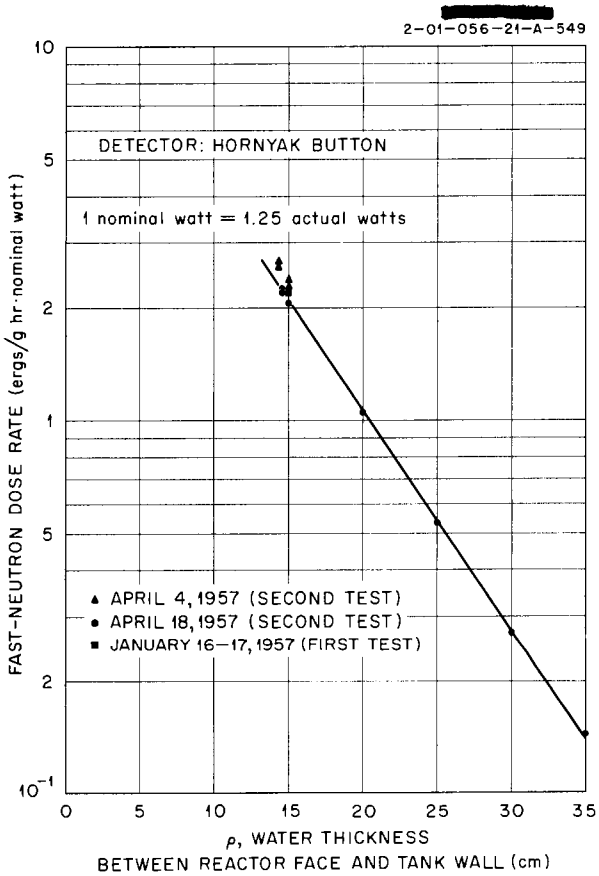

Fig. 6.2.2. Fast-Neutron Dose Rates at the Point of Intersection of a Line Coincident with the J-57 Axis and a Line Coincident with the Reactor Axis as a Function of the Reactor Shield Thickness (Tests I and II, Phase I, Engine Not Present).

It has been shown that a 5-mil-thick gold foil is essentially black to gold resonance neutrons (5 ev). Hence the activation in the front foil of the stack was due to both resonance and nonresonance neutrons. The activation of the middle foil was due to nonresonance neutrons only, if slowing down within the foil is ignored. The activation in the second foil was corrected for nonresonance flux absorption in the first foil, and the difference in the saturated specific activities of the first and second foils was taken to be due entirely to gold resonance neutrons. Then, at saturation the resonance flux should be equal to the disintegration rate induced by resonance neutrons. This flux is plotted in the lower curve in Fig. 6.2.4 as a function of the distance from the engine tailpipe. An average nonresonance flux depression of 8.8% through the front foil was obtained by separate experiments. The third, or back foil, was used in the foil stack only to prevent absorption of back-scattered resonance neutrons. A rather large error, approximately ±50%, results from taking the difference between the activities of the first and second foils, inasmuch as the magnitudes of the activities are nearly equal.

The thermal-neutron flux at each position was determined from the difference in the activity of the front foil in the stacked foil and that in a cadmium-covered gold foil exposed at a position adjacent to the stacked foil. In this case the thermal-neutron flux was taken to represent neutrons of less energy than the cadmium cutoff (0.4 ev). Since the low-energy portion of the neutron spectrum is unknown, the average gold cross section (52 barns) between 0.025 and 0.40 ev was used in calculating the thermal-neutron flux. The results are plotted in the upper curve in Fig. 6.2.4. The estimated error is less than 50%.

Measurements During Irradiation (Phase II)

During phase II, measurements were made on the surface of the engine while it was being irradiated. These include measurements with Pu^{239}, Np^{237}, U^{238}, and S threshold detectors to determine the total neutron flux above energy thresholds of 6.0 kev, 0.75 Mev, 1.5 Mev, and 2.9 Mev, respectively. In addition, stacked gold

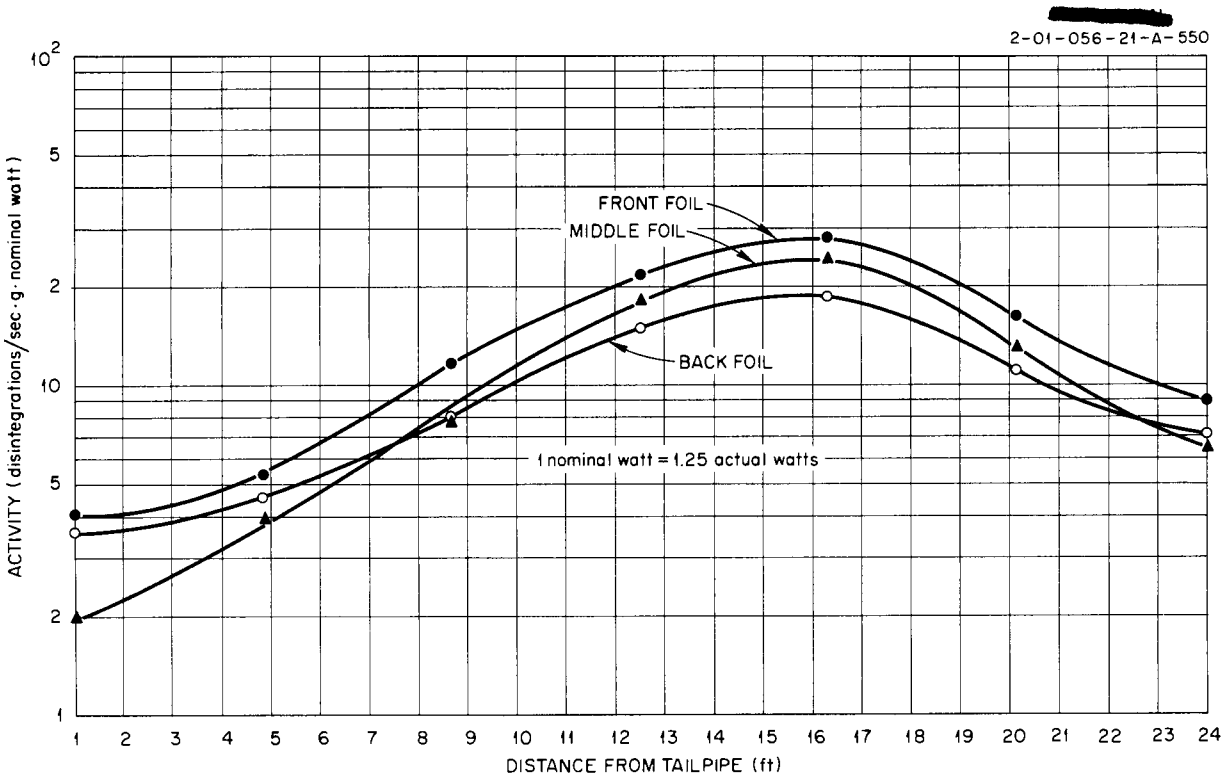

Fig. 6.2.3. Saturated Specific Activities of Gold Foils Exposed Along a Line Coincident with the J-57 Engine Axis (Test II, Phase I, Engine Not Present).

foils were used to determine the 5-ev neutron flux. The agreement of these individual threshold detector measurements (not shown here) with similar measurements taken during the first test[2] was within experimental error. The integrated fast-neutron tissue-equivalent dose to which the engine was exposed was calculated in the manner outlined previously[2] and is plotted in Fig. 6.2.5 as a function of the distance from the tailpipe. Also, one measurement taken with a Hornyak button detector at a location identical to that of one of the threshold detectors is shown for comparison.

In addition to the threshold detectors, gold wires were strung parallel with the engine axis on both sides of the engine during the 50-hr exposure. The wire was wrapped with 20-mil-thick cadmium foil at 1-ft intervals and with 5-mil-thick gold foils midway between the cadmium wrappers. The cadmium-covered wire detected epicadmium neutrons, the gold-covered wire approximated a $1/v$ detector, and the bare wire acted as a detector of all neutrons of energies ranging up to about 200 ev. The count rates obtained with the wires on both sides of the engine are plotted as functions of the distance from the tailpipe in Fig. 6.2.6.

Measurements Following Engine Irradiation (Phase III)

After termination of the 50-hr exposure, the engine was removed from the vicinity of the reactor for the phase III measurements. The gamma-ray dose rate from neutron-induced activation of the materials in the engine was observed as a function of time at various locations around the engine. Some measurements were made with a "cutie-pie" survey type of ion chamber at points ranging from surface contact up to 20 ft from the engine axis. These measurements were within the experimental error of those obtained after the first engine

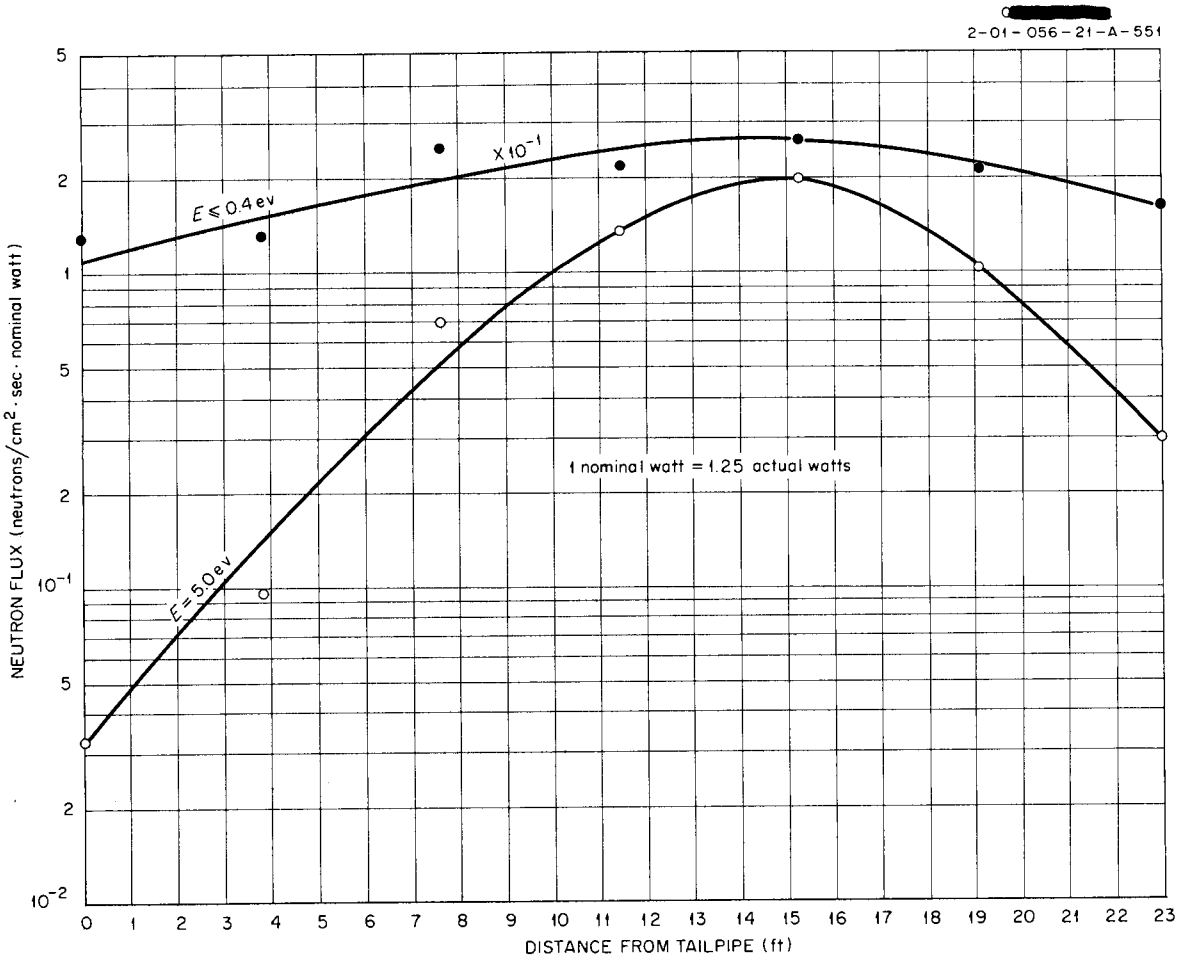

Fig. 6.2.4. Neutron Fluxes Along a Line Coincident with the J-57 Engine Axis (Test II, Phase I, Engine Not Present).

irradiation.[2] In addition, more quantitative data were taken with an anthracene crystal, a d-c integrator, a logarithmic count-rate meter, and a Brown recorder. The decay gamma-ray dose rate measured with this crystal 5 ft 2¾ in. from the point of highest intensity (that is, from the point which had been opposite the center of the reactor during the exposure) as a function of time after reactor engine shutdown is shown in Fig. 6.2.7. The crystal was mounted on a track and dolly mechanism so that it could be moved along lines both parallel with and perpendicular to the engine axis in order to obtain the radial and axial distribution of the gamma-ray field. The Brown recorder signal was fed into a variplotter to record the gamma-ray dose rate as a function of position. The results of these measurements are shown in Figs. 6.2.8 and 6.2.9.

A sample of the engine oil was examined after the irradiation for induced radioactivity. The 3- by 3-in. sodium iodide crystal and 20-channel analyzer system described previously[2] was used to obtain pulse-height spectra of nuclear radiation emanating from the oil sample. The pulse-height spectra, two of which are shown in Fig. 6.2.10, seemed to suggest a Na^{24} gamma-ray spectrum[2] (E = 2.75 and 1.38 Mev) superimposed upon a continuous beta-ray spectrum. Half-life and beta-ray absorption studies led to identification of the responsible isotopes as Na^{24} and P^{32}. The

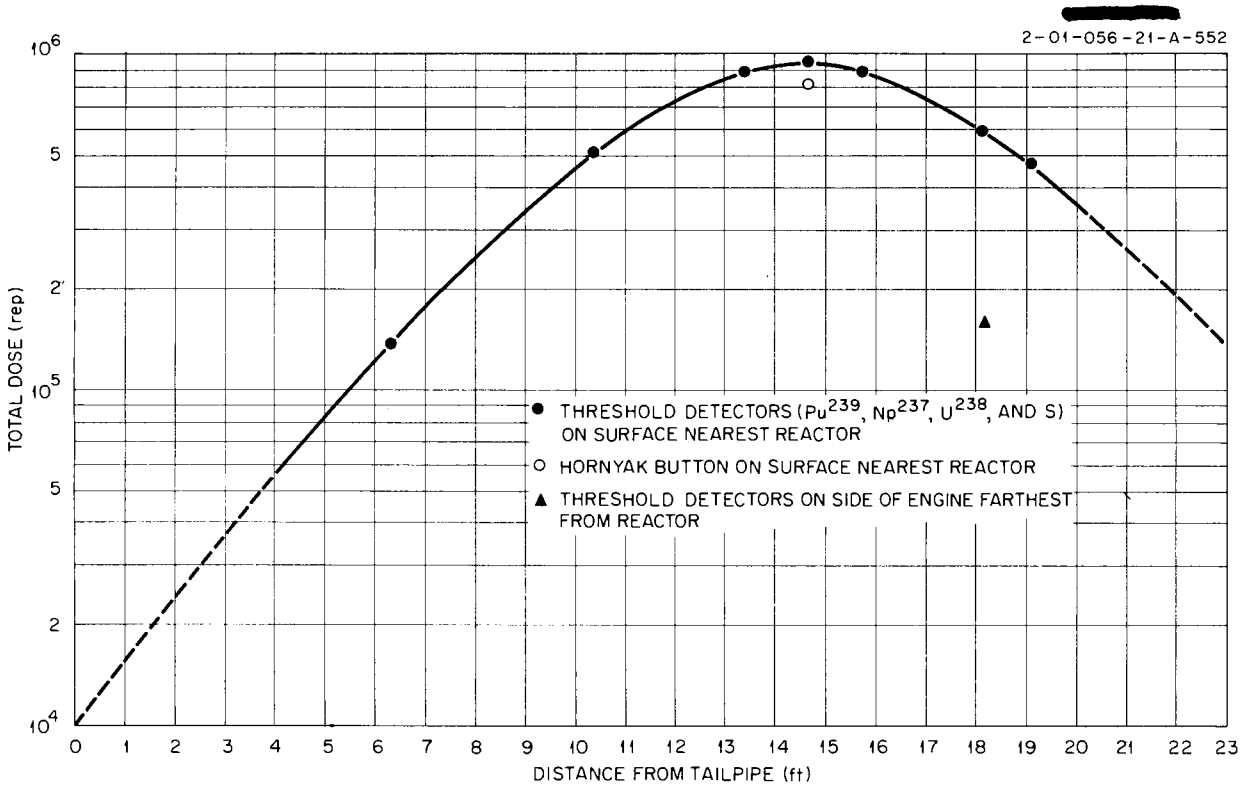

Fig. 6.2.5. Total Fast-Neutron Dose Exposure of the Surface of the J-57 Engine as a Function of Distance from the Tailpipe (Test II, Phase II).

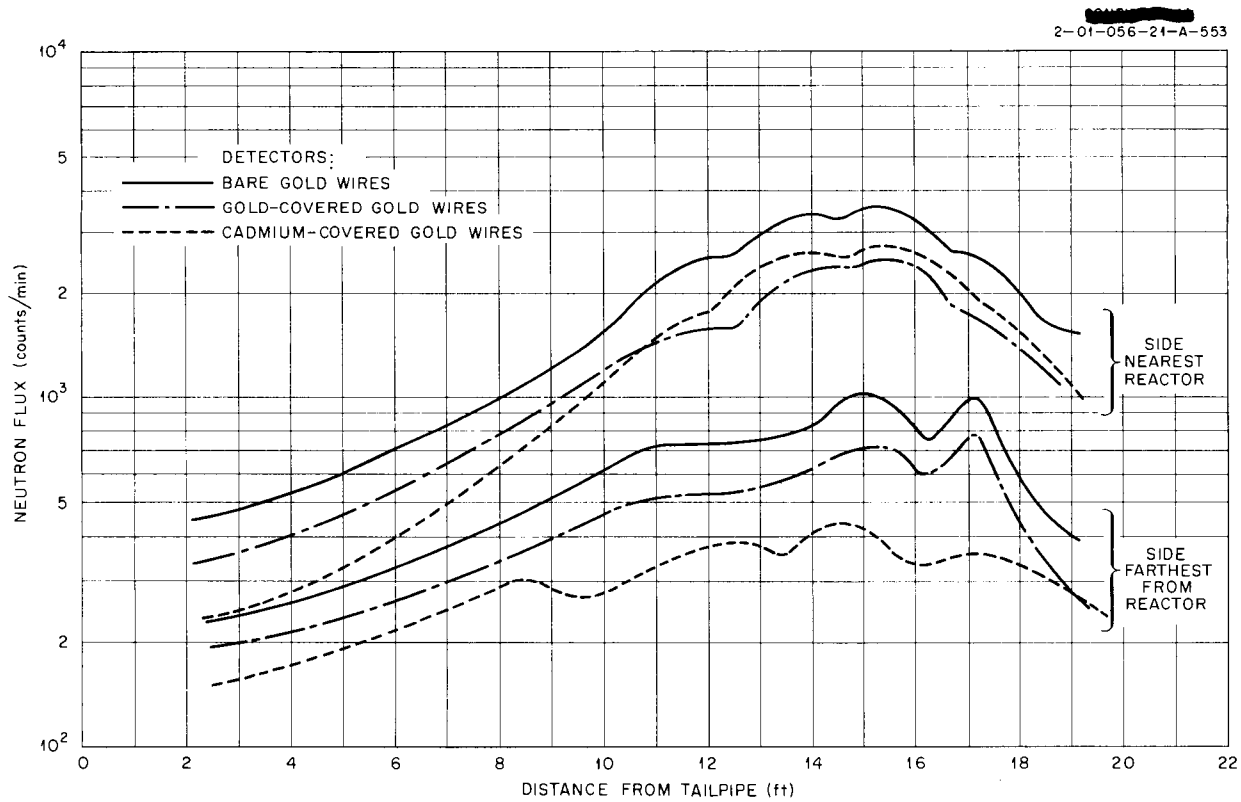

Fig. 6.2.6. Neutron Fluxes on the Surface of the J-57 Engine During Irradiation as a Function of Distance from the Tailpipe (Test II, Phase II).

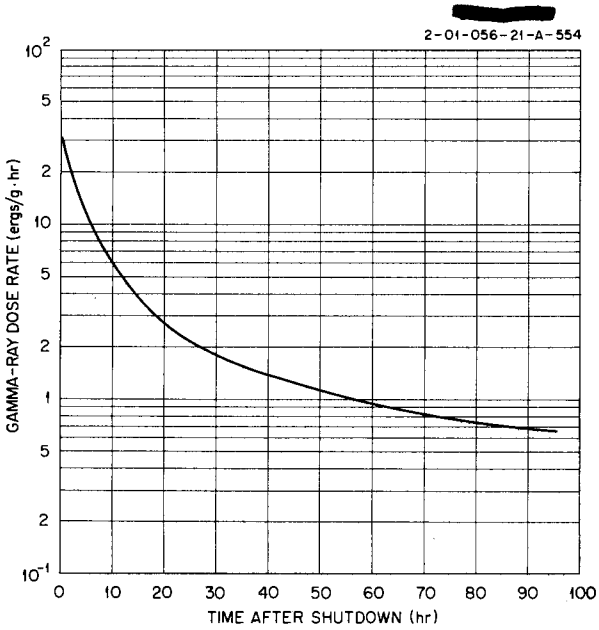

Fig. 6.2.7. Decay Gamma-Ray Dose Rate 5 ft $2\frac{3}{4}$ in. from the Point of Highest Intensity on the Surface of the J-57 Engine (Test II, Phase III).

saturated specific activities were calculated to be 2.17×10^5 dpm/ml for P^{32} and 4.54×10^2 dpm/ml for Na^{24}.

DETERMINATION OF THE POWER OF THE TOWER SHIELDING FACILITY REACTOR

F. N. Greene[3] C. R. Fink[3]
W. E. Price[1]

The power of the Tower Shielding Facility (TSF) reactor is one of the variables in every shielding experiment, since the actual power for a specified nominal power is known to change with time. Thus interpretation of test data on a dose-per-watt basis taken over any appreciable time span must include an evaluation of the variation in the power. In the past, calorimetric power determinations have been made at about six-month intervals and the results obtained have varied as much as 24%. Also, there has been an indication that the power was gradually increasing with time. In order to collect sufficient data for a statistical analysis of the error and to determine possible trends, additional heat-power experiments were conducted weekly during the month of March and bimonthly thereafter.

Experimental Technique

The reactor power was determined by measuring the heat output in a simple calorimetric experiment. In order to provide the least variant environment for the apparatus during the run, the reactor tank was placed in the pool and the pool was drained to a level below the tank. The tank contained a predetermined number of pounds of moderator water, and a propeller-type agitator was placed in the water to provide stirring action to maintain a uniform temperature of the water throughout the tank. Earlier experiments had indicated that this amount of agitation was sufficient.[4] Measurements of the water level in the reactor tank before and after the power run, together with thermal expansion calculations for both the water and the tank, showed that the amount of water lost by evaporation was negligible.

Five type J(IC) iron-constantan thermocouples mounted on a vertical rod about 3 ft from the reactor were placed in the reactor tank at various depths. Thermocouple readings were taken with a potentiometer and a Leeds & Northrup galvanometer. The thermocouple calibration was 0.0523 mv/°C over the range of water temperatures recorded.

Prior to reactor startup, the agitator was operated until thermocouple readings indicated that temperature equilibrium existed in the tank. The reactor was then brought to operating power (400 kw, nominal power) on a short period so that heat input during this period would be negligible. Thermocouple readings were taken at 10-min intervals for exactly 2 hr, at which time the reactor was scrammed. The readings were continued for 2 hr to obtain a cooling curve. Ambient air temperatures were also recorded at $\frac{1}{2}$-hr intervals.

[3] On assignment from Glenn L. Martin Co.

[4] L. B. Holland and J. L. Hull, *Phys. Semiann. Prog. Rep. Sept. 10, 1954*, ORNL-1820, p 9.

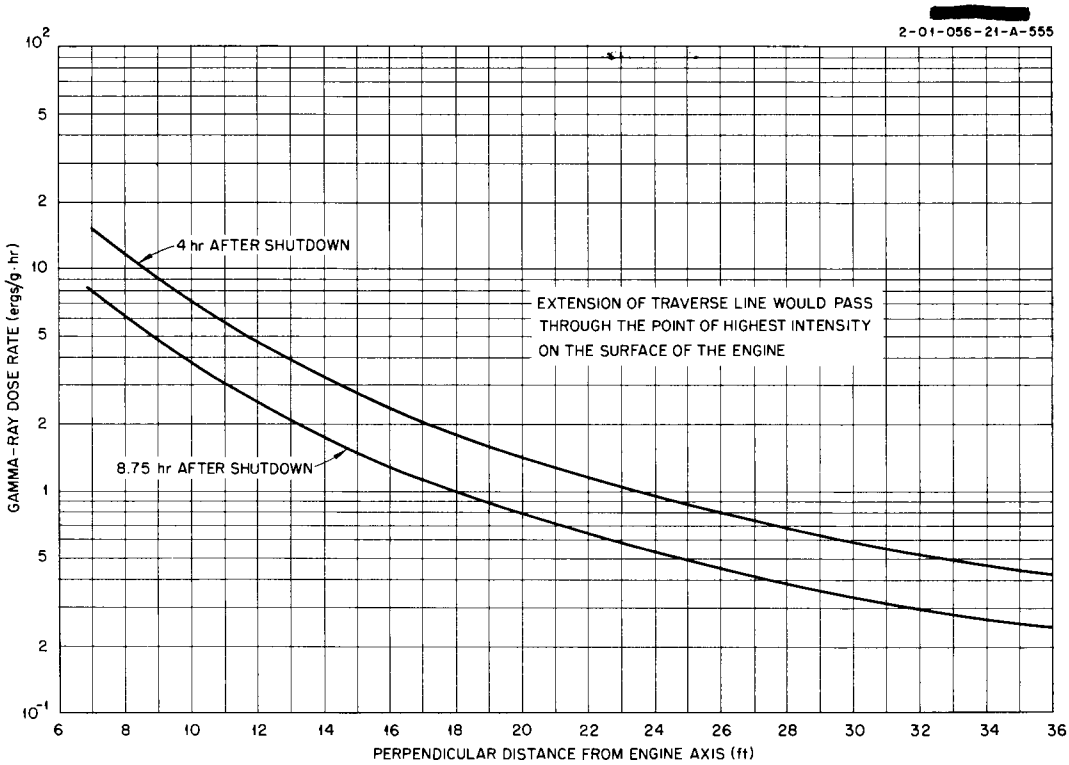

Fig. 6.2.8. Gamma-Roy Dose Rates 4 and 8.75 hr After Reactor Shutdown Along a Line Perpendicular to the Axis of the J-57 Engine (Test II, Phase III).

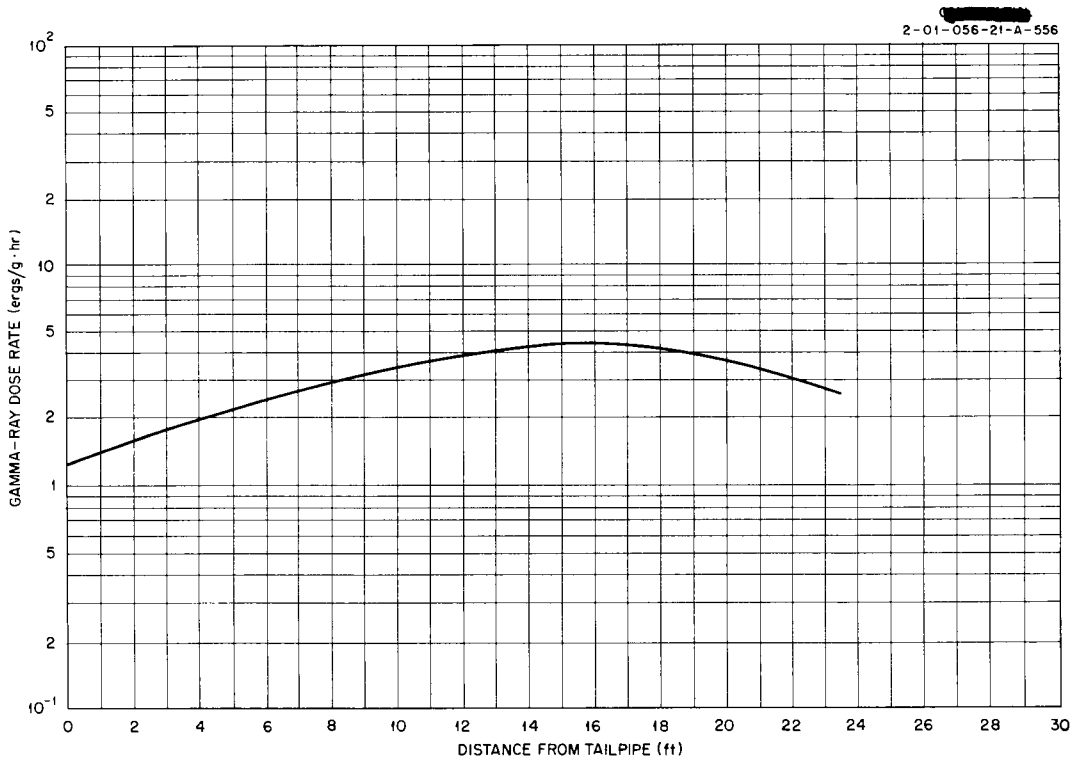

Fig. 6.2.9. Gamma-Ray Dose Rate 6 hr After Reactor Shutdown Along a Line Parallel to and 10 ft 1 in. from the J-57 Engine Axis (Test II, Phase III).

[redacted]

2-01-056-21-A-557

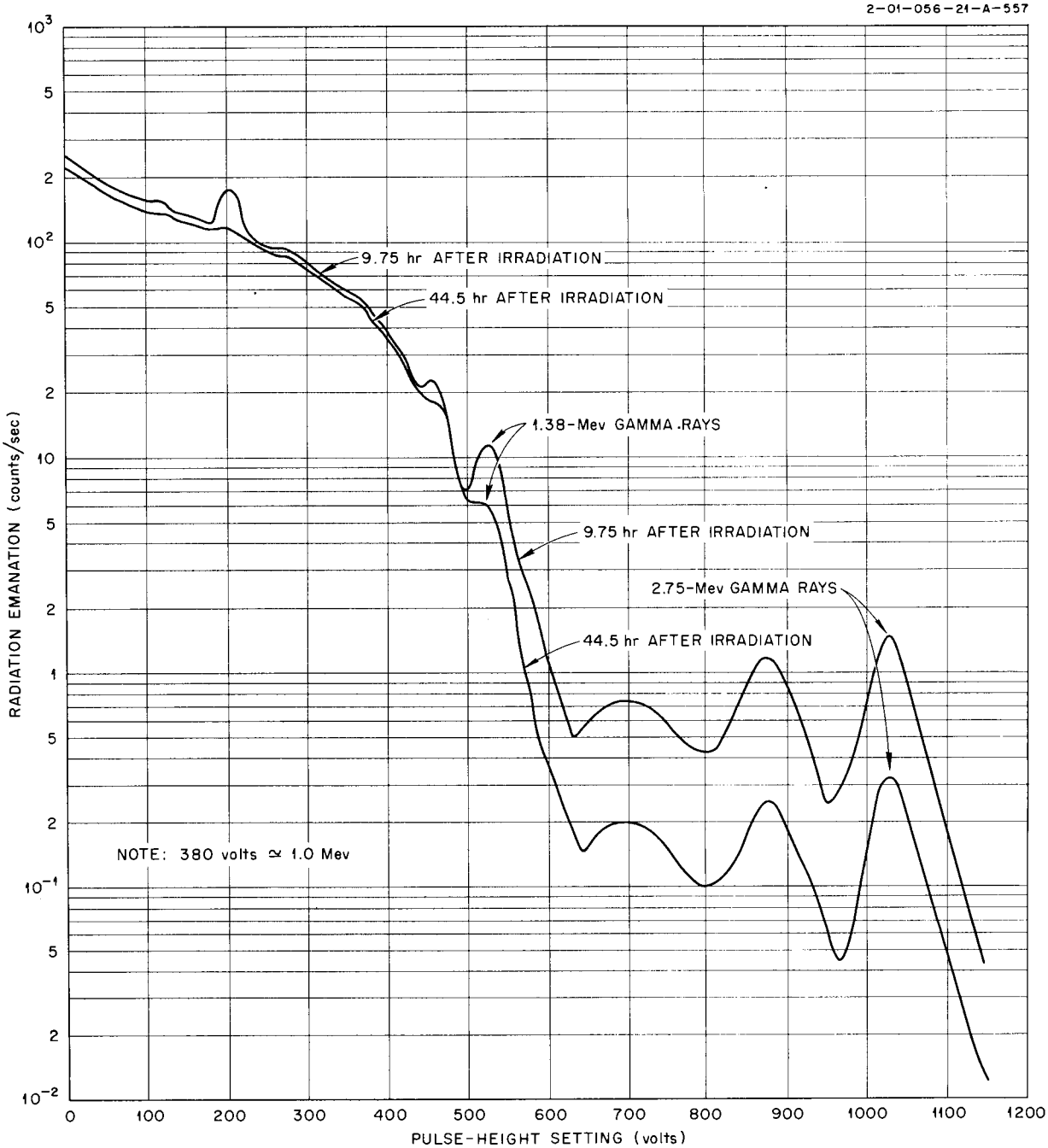

Fig. 6.2.10. Pulse-Height Spectra of Decay Radiation Emitted from J-57 Engine Oil Samples 9.75 and 44.5 hr After Irradiation (Test II, Phase III).

Method of Calculation

The masses of the tank, reactor, and water which absorbed the heat generated by the operating reactor were known. For calculational purposes these weights were converted to an effective total water weight of 73,500 lb. Thus for each degree Fahrenheit of temperature rise, 73,500 Btu of heat was absorbed by the entire system, which is equivalent to 38.8 kwhr for each degree centigrade of temperature rise. Thus, if the rate of temperature rise in the system during an operating (or heating) cycle were determined and if appropriate corrections were made for cooling during the heating cycle, the actual power of the reactor could be calculated.

Two methods were used to obtain the rate of temperature rise of the system during the heating cycle. In the first method, measurements with each of the five thermocouples were plotted as a function of time and the plots were fitted with straight lines. The slope of each straight line was considered to be the rate of temperature increase of the system as indicated by that thermocouple.

In a second method, the straight-line fit to each set of thermocouple data was corrected to account for the afterheat from the reactor after shutdown. That is, after the reactor was shut down, the temperature of the system continued to increase for a short period, though at a slower rate, before it began to fall steadily. This resulted from the temperature of the reactor proper being higher than that of the surrounding water at shutdown. In this second method of calculation a straight-line extrapolation of the cooling curve was made back to the time at shutdown to obtain a corrected temperature at shutdown. The slope of the straight line between the initial temperature and the corrected final temperature was then considered to be the rate of temperature increase in the system.

It is to be noted that the over-all temperature difference used to determine the slope, or rate of temperature increase, in either method was obtained simply by subtracting the initial temperature of the system from the final temperature, with no corrections being made for heat loss. A precise determination of the heat loss was considered unnecessary since the loss at the maximum temperature was only 5% of that being generated. An approximate correction was made to the heating rate, however, in which it was assumed that the cooling rate during the heating cycle varied linearly with the temperature difference. The corrected slope was then used to obtain the reactor power, P, according to the following formula:

$$P(\text{kw}) = 38.8 \left[S_1 + \left(\frac{\frac{T_F + T_i}{2} - T_a}{T_F - T_a} \right) S_2 \right],$$

where

S_1 = rate of temperature increase during the heating cycle, °C/hr,

S_2 = rate of temperature decrease during the cooling cycle, °C/hr,

T_F = measured water temperature at shutdown for method 1; extrapolated water temperature at shutdown for method 2, °C,

T_i = water temperature at startup, °C,

T_a = ambient air temperature, °C.

No correction was required for the heat added to the system during reactor startup and shutdown.

Results and Discussion

A summary of the results of the power determinations by both methods 1 and 2 for all five thermocouples over a period of weeks is given in Table 6.2.1. A plot of the data (Fig. 6.2.11) clearly indicates the trend toward increasing power with time. In view of this, application of statistical analysis to the results over too long a time period would be unrealistic. However, analyses of the results obtained from March 1 to May 10 showed that all values fell within the limits of statistical variation, with a probable error of ±1.6%. Although no definite conclusions concerning the course of the trend can be made at this time, there are indications from measurements of the thermal-neutron flux in a single fuel element, that the power distribution does change with time. A re-evaluation of present experimental techniques and assumptions made in the calculations, along with a recalibration of measuring and recording devices, will be made in order to determine sources of correctable errors.

Table 6.2.1. Summary of Actual Power Determinations by Calorimetric Experiments for the TSF Reactor Operating at a Nominal Power of 400 kw

Date	Reactor Power (kw)					
	Thermocouples					
	No. 1	No. 2	No. 3	No. 4	No. 5	Average
			Method 1			
4-30-56						336
5-16-56						341
8-17-56						448
1-31-57						500
3-1-57	508.2	512.1	528.21	495.7	500.2	508.9
3-4-57	521.8	518.7	516.5	518.0	517.3	518.5
3-8-57	499.4	510.6	504.7	500.3	495.0	502.0
3-14-57	521.6	512.5	508.3	510.1	518.0	514.1
3-22-57	521.7	526.0	542.5	514.9	513.5	523.8
4-26-57	520.3	502.8	511.1	529.3	512.8	515.3
5-10-57	520.4	558.1	504.8	517.1	503.8	520.8
			Method 2			
3-1-57	497.5	498.8	501.2	498.3	500	499.2
3-4-57	527.2	521.1	514.3	514.3	505.4	516.5
3-8-57	506.5	507.2	508.0	506.5	502.8	506.2
3-14-57	510.5	518.8	511.2	512.3	511.5	512.9
3-22-57	531.7	532.6	532.0	531.1	525.4	532.2
4-26-57	527.6	530.6	524.7	531.1	525.4	527.9
5-10-57	522.8	548.5	515.5	541.3	516.7	529.0

Auxiliary Methods of Determining Power Linearity

Calorimetric experiments as a regular method of determining power linearity would be impractical because of the length of time required, as well as the inherent inaccuracies associated with the determinations at low power levels. As an alternative, the linearity of the TSF reactor was determined by measuring the thermal-neutron flux at a constant distance from the reactor while varying the reactor power over the range of 4 to 400 kw. The fission chamber used for these measurements was placed in the reactor tank at a distance from the reactor such as to give an adequate count rate for good statistical results at low powers and, in addition, to keep the count rate at a maximum of about 100,000 counts/min at full power. This was necessary because of the excessive error introduced at higher count rates as a result of the resolution time on the chamber. The error at a count rate of 100,000 counts/min was approximately 0.67%.

The results of the fission-chamber measurements are tabulated in Table 6.2.2, along with corrected results for higher count rates. The values given are mean values of several measurements, and the probable errors are indicated. A plot of the count

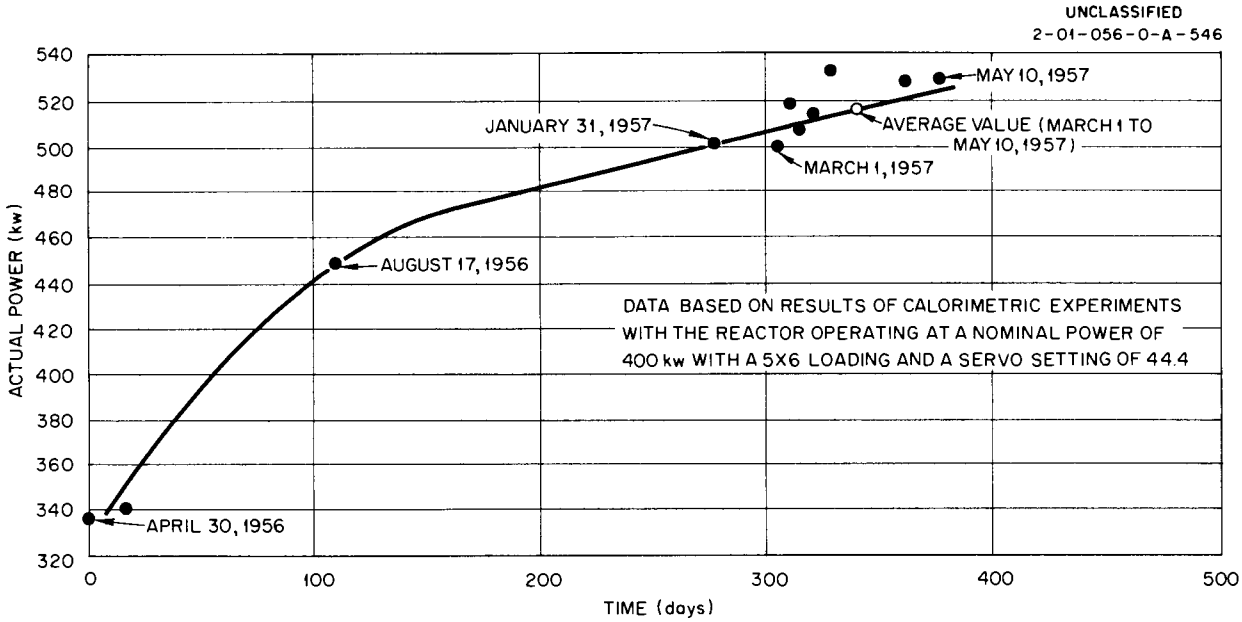

Fig. 6.2.11. Actual Power Variation of TSF Reactor from April 30, 1956 to May 10, 1957.

Table 6.2.2. TSF Reactor Power Linearity Measurements with the Fission Chamber at a Constant Distance from the Reactor

Nominal Power (kw)	N, Measured Mean Count Rate* (counts/min)	N_0, Corrected Mean Count Rate* (counts/min)	Probable Error of N (counts/min)	N_0 per Nominal Watt
4	1,161	1,161	10	290 ± 3
10	2,920	2,921	16	292 ± 2
20	5,708	5,710	23	286 ± 1
40	11,548	11,557	32	289 ± 1
100	29,717	28,772	51	288 ± 1
200	57,408	57,630	72	288 ± 0
400	114,564	115,451	102	289 ± 0

*It can be shown that the ratio of the measured to the actual count rate decreases with increasing count rates according to the relationship:

$$N = N_0\left(1 - \frac{\lambda N}{60}\right),$$

where N is the measured number of counts per minute, N_0 is the actual (or corrected) number of counts per minute, $\lambda N/60$ is the dead-time fraction, and λ is the resolution time of the fission chamber (taken as 4 μsec for the chamber used).

rate as a function of the nominal reactor power is given in Fig. 6.2.12.

A second experimental determination of the power linearity was made by measuring the gamma-ray dose rate in air at a distance 64 ft from the center of the reactor tank. Since a constant water thickness, ρ, in front of the reactor could not be maintained, the resulting gamma-ray curve shown in Fig. 6.2.12 presents the total gamma-ray dose rates at each power normalized to $\rho = 15$ cm. Both these auxiliary methods show the power to be linear throughout the full range of power.

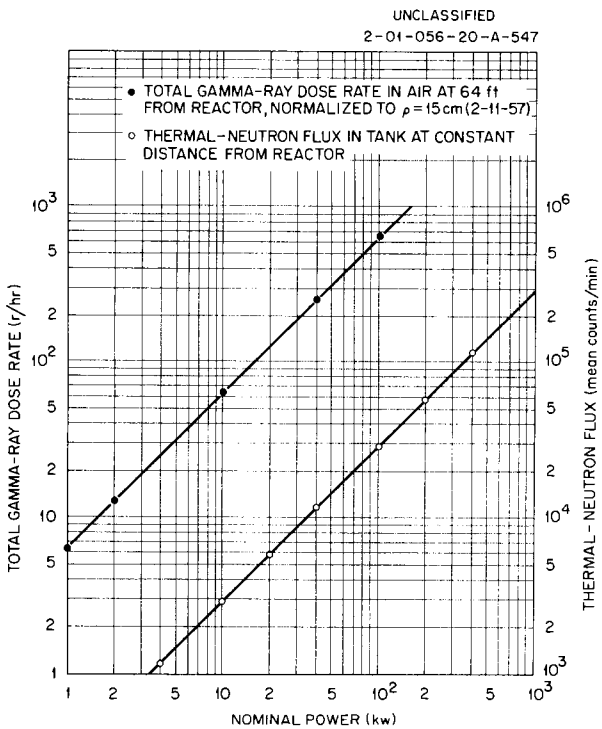

Fig. 6.2.12. Gamma-Ray Dose Rate and Thermal-Neutron Flux Measurements as a Function of the Nominal Power of the TSF Reactor.

REPRODUCIBILITY OF TSF DATA

F. N. Greene[5] V. R. Cain

An experimental program was initiated to determine the accuracy with which TSF data could be reproduced. The ultimate aim in this series of experiments was to determine the individual experimental errors for each of the variables which affect the final dose data in order to establish a composite experimental error.

The main effort of the program was devoted to geometrical measurements taken at zero power with the reactor at ground level. Since the reactor power determination discussed in the preceding paper showed the power to be linear over the full range, with a slight tendency to increase with time, a study of the power variable was omitted under the assumption that the variation would be negligible over the short period in which the data were taken. The reproducibility of all the other variables affecting dose rates was investigated by taking a sufficient number of on-the-ground measurements and statistically evaluating the results.

The culmination of the program was a series of repetitive in-air measurements of the fast-neutron dose with the triple-chamber fast-neutron dosimeter at a position 64 ft from the reactor. Three combinations of the reactor angle θ and the water thickness ρ in front of the reactor were chosen as the most critical combinations for a θ traverse, that is, the combinations in which an error in the measurement of θ would have the most effect on the measured dose rate. The minimum values of ρ were used in order to obtain good count rates, and the gamma-ray field was kept below a dose rate of 2 r/hr. The points measured were as follows:

Point	θ (deg)	ρ (cm)
1	30	60
2	60	40
3	90	20

Nine readings were taken at each point over a period of a week by different operators. The results are tabulated in Table 6.2.3. Statistical analysis shows that the data for point 2 are critical, with a probable error of ±2.2%. Since this point is on the steepest slope of the θ traverse, most of the error can be attributed to the probable error of ±0.2 deg in the measured value of θ, as found from the analysis of the data. The probable errors of the data for points 1 and 3 are ±1.8 and 0.8%, respectively. This indicates that if three times the probable error were used, 95% of the TSF data would fall within ±6.6% of the mean.

[5] On assignment from Glenn L. Martin Co.

Table 6.2.3. Fast-Neutron Dose Rates in Air 64 ft from the TSF Reactor

Reading No.	Fast-Neutron Dose Rate (ergs·g/w)		
	Point 1	Point 2	Point 3
	$\times 10^{-4}$	$\times 10^{-4}$	$\times 10^{-4}$
1	1.03	3.00	6.19
2	1.06	2.92	6.03
3	0.99	2.82	6.02
4	0.99	2.82	6.08
5	1.03	2.80	6.02
6	0.99	2.79	5.98
7	0.99	3.01	6.02
8	0.99	2.87	6.06
9	1.01	3.01	5.95
Av	1.01	2.89	6.04

DEVELOPMENT OF THE HORNYAK BUTTON AS A FAST-NEUTRON DOSIMETER

F. J. Muckenthaler

It was reported previously[6] that the Hurst type of fast neutron dosimeter, which is commonly used for fast-neutron dose measurements at the ORNL shielding experiment facilities, is limited by several features and that efforts were being made to develop a new dosimeter with a Hornyak button[7] as the detector. (The Hornyak button consists of a homogeneous mixture of fine Lucite and ZnS powders.) At the time of the previous statement the response of various Hornyak buttons to fast neutrons from a Po-Be source and from the TSF and BSF reactors had been examined. In addition, some preliminary tests had been performed in which the response of the button to monoenergetic neutrons produced by the ORNL 5.5-Mev Van de Graaff generator was compared directly with the response of the Hurst type of dosimeter. The Hurst type of dosimeter serves as a good basis for comparisons because the neutron dose rate it measures is approximately the dose rate absorbed in tissue.

Further tests have now been performed to compare the responses of the various Hornyak buttons with that of the dosimeter. For these tests, monoenergetic neutrons produced by a tritium-gas target bombarded with protons from the Van de Graaff were used as the source. In order to ensure that both detectors had an incident neutron flux of the same energy, they were placed in the same horizontal plane, each located at an angle of 15 deg from the generator beam with their centers of detection the same distance from the target. The counting time for each run was based on a predetermined beam current, as is necessary for the calculation of the neutron flux for each energy interval. The ratio of the dose rate obtained with the dosimeter to that obtained with the Hornyak button was then plotted as a function of the neutron energy.

It was necessary to keep the over-all gain of the dosimeter constant for each run for a comparative evaluation of the results. This was accomplished by placing the dosimeter in a 2-r/hr Co^{60} gamma-ray field and adjusting the gain of the A-1 amplifier until 25 counts/min were observed for a predetermined high voltage and a pulse-height selector reading of 6 v. A precision pulser was used to check and adjust the electronic gain of the dosimeter prior to each measurement at different neutron energies. The Hornyak buttons were also biased to give 25 counts/min at a pulse-height reading of 6 v when placed in a 2-r/hr gamma-ray field. For convenience only, the electronic gain was kept constant, and the high voltage was changed to give the bias. With the gamma-ray source removed, the two detectors were calibrated against a Po-Be source of known intensity.

In the earlier tests[6] it was shown that the ratio of the dose rates from the two detectors varied from unity to a substantial extent only at neutron energies below about 1 Mev. Since this was the energy region of interest, the range of neutron energies measured by each button was kept below about 2.2 Mev. This reduced the experimental time required for tests of each button and permitted a larger number of buttons to be tested.

The Hornyak buttons used in this series of tests contained 25-μ-dia and 3- to 5-μ-dia ZnS particles.

[6] F. J. Muckenthaler, *Appl. Nuclear Phys. Ann. Prog. Rep. Sept. 10, 1956*, ORNL-2081, p 199.

[7] W. F. Hornyak, *Rev. Sci. Instr.* **23**, 264 (1952).

The lowest concentration of ZnS used in the buttons containing 25-μ-dia particles was 50 parts by weight in 70 parts of Lucite, since earlier data for lower concentrations indicated that as the amount of ZnS was increased to 50 parts and the thickness of the button was decreased to 0.020 in., the response to low-energy neutrons increased. The concentrations of ZnS used in the buttons containing 3- to 5-μ-dia particles were varied from 0.4 to 50 parts by weight in 70 parts of Lucite, and various button thicknesses were used. The minimum button thickness was about 0.020 in.

The ratios of the dose-rate response of the dosimeter to the response of various Hornyak buttons containing the 25-μ-dia ZnS particles are shown in Figs. 6.2.13 through 6.2.16. For ZnS concentrations of 100 and 150 parts, the low-energy response increased as the button thickness decreased. For a concentration of 250 parts, however, the response in the low-energy region decreased. This reversal can be attributed to cracks in the Lucite-ZnS crystal resulting from difficulty in machining a crystal with large concentrations of ZnS. A summary of the best response obtained with buttons of each concentration of 25-μ-dia ZnS particles is given in Fig. 6.2.17. There appears to be little difference between the buttons with 50 and 100 parts of ZnS, but above this concentration the dose-rate ratio stays above one, even at neutron energies of 2 Mev. This appears to confirm the earlier observation[6] that the optimum ZnS concentration for maximum low-energy response is between 50 and 100 parts by weight in 70 parts of Lucite.

The results of tests with buttons containing 3- to 5-μ-dia ZnS particles are shown in Figs. 6.2.18 through 6.2.22. For ZnS concentrations of 20, 50, and 100 parts, the low-energy response increased as the button thickness decreased. Changing the thickness of the button appeared to have no effect for ZnS concentrations of 0.4 to 5 parts. A summary of the data (Fig. 6.2.23) shows that for concentrations of 0.4 to 4 parts by weight, the dose-rate ratio is approximately one at low neutron

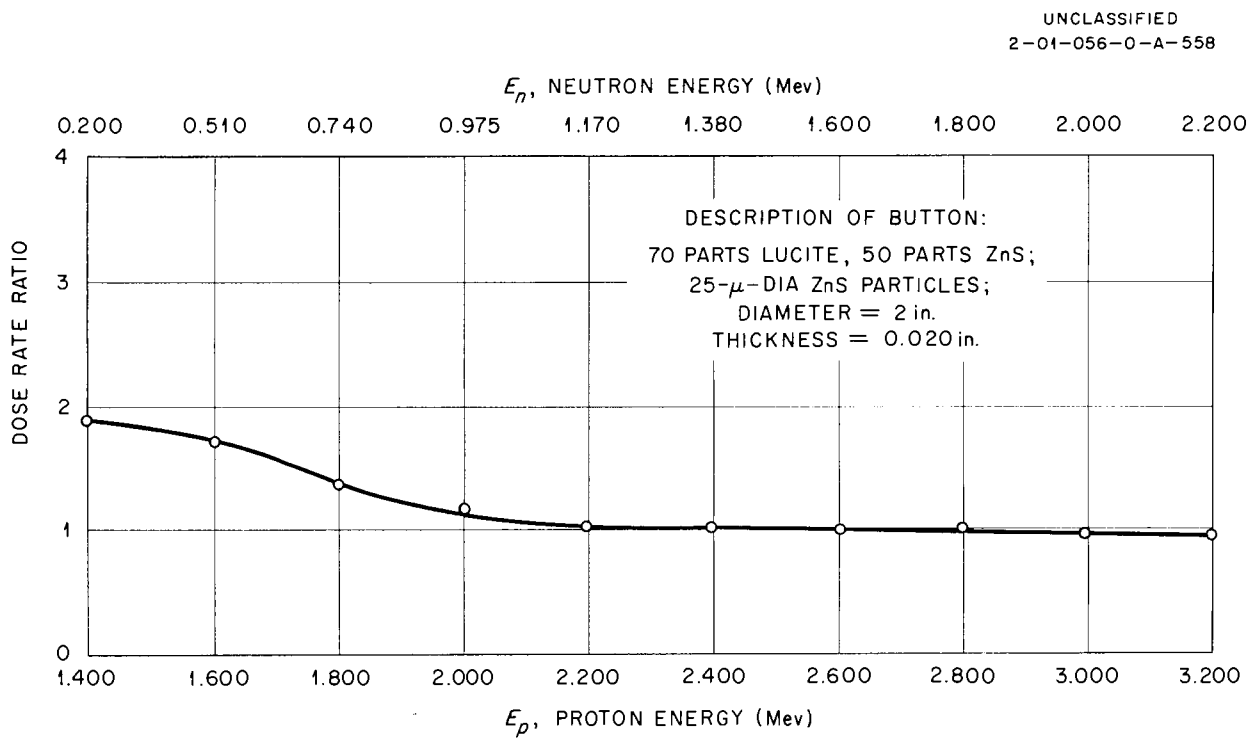

Fig. 6.2.13. Ratio of the Dose-Rate Response of the Dosimeter to the Response of the Hornyak Button to Neutrons from the (p,t) Reaction (Van de Graaff Generator).

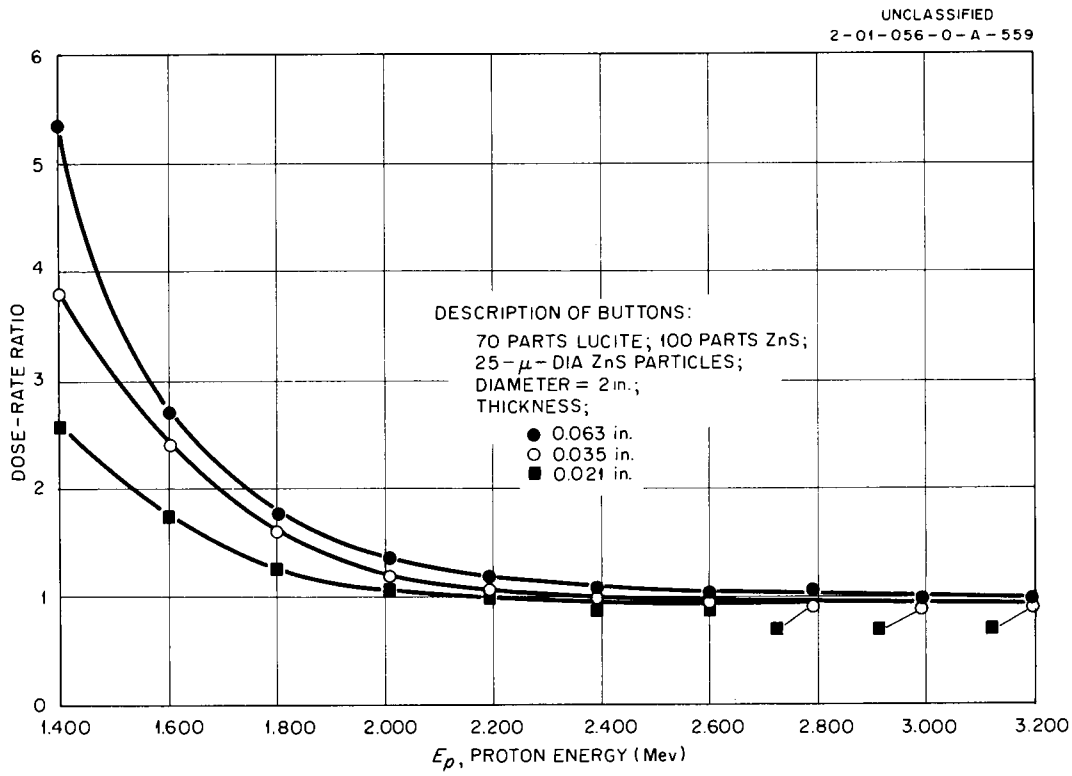

Fig. 6.2.14. Ratio of the Dose-Rate Response of the Dosimeter to the Response of Various Hornyak Buttons to Neutrons from the (*p*,*t*) Reaction (Van de Graaff Generator).

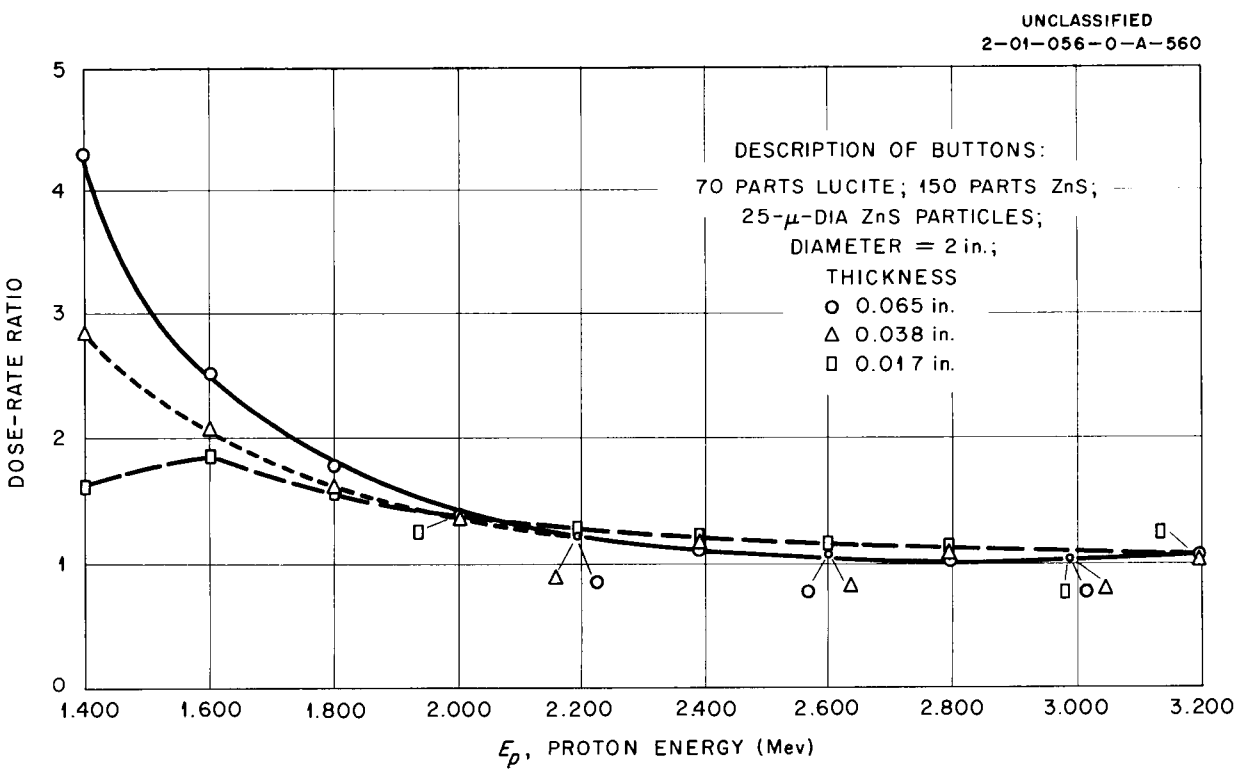

Fig. 6.2.15. Ratio of the Dose-Rate Response of the Dosimeter to the Response of Various Hornyak Buttons to Neutrons from the (*p*,*t*) Reaction (Van de Graaff Generator).

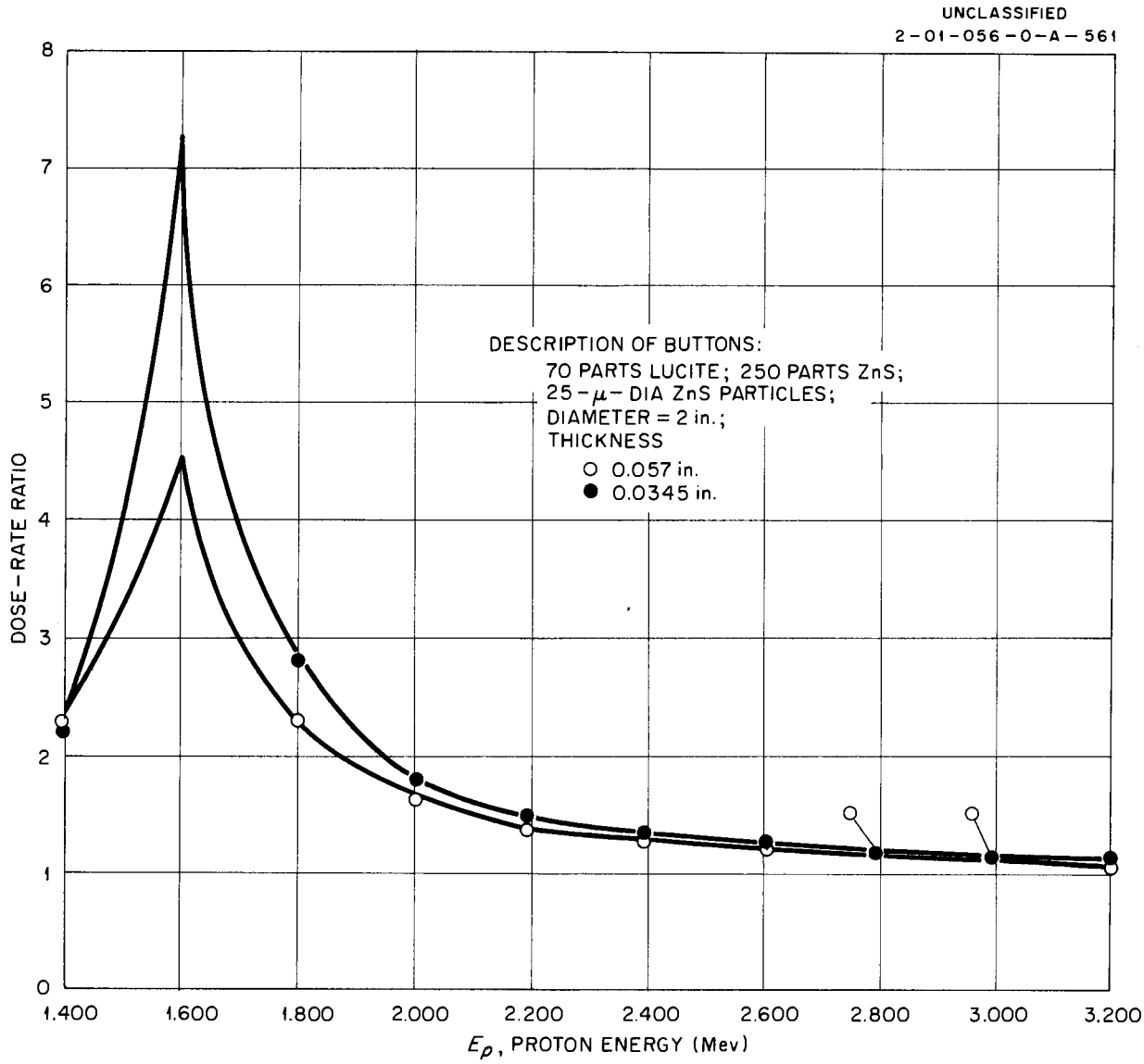

Fig. 6.2.16. Ratio of the Dose-Rate Response of the Dosimeter to the Response of Vorious Hornyok Buttons to Neutrons from the (p,t) Reaction (Van de Graaff Generator).

energies and less than one for slightly higher energies. As the ZnS concentration was increased, the low-energy response decreased.

In conjunction with the above measurements, other data were obtained for comparing some of the buttons with the dosimeter for measurements beyond several reactor shield configurations at the TSF. For these measurements the detectors were placed in air 64 ft from the reactor tank. The reactor was positioned along the tank-detector axis 60 cm from the tank wall to give a hardened direct beam. Other measurements were made with the reactor in a position 90 deg from the detector-tank axis and 20 cm from the tank wall. This arrangement resulted in a neutron spectrum at the counter that had a large low-energy air-scattered component. Comparisons of the response of the two detectors indicate a trend similar to that found with monoenergetic neutrons. For the air-scattered spectrum, the buttons containing 25-μ-dia particles gave dose-rate readings that were lower than the readings of the dosimeter by about 10%. For the hard direct beam, the dose rates observed were almost equal. Insufficient measurements were taken with the buttons containing 3- to 5-μ-dia particles to permit comparisons with the response of the dosimeter at this time; however, there is an indication that these buttons give higher dose-

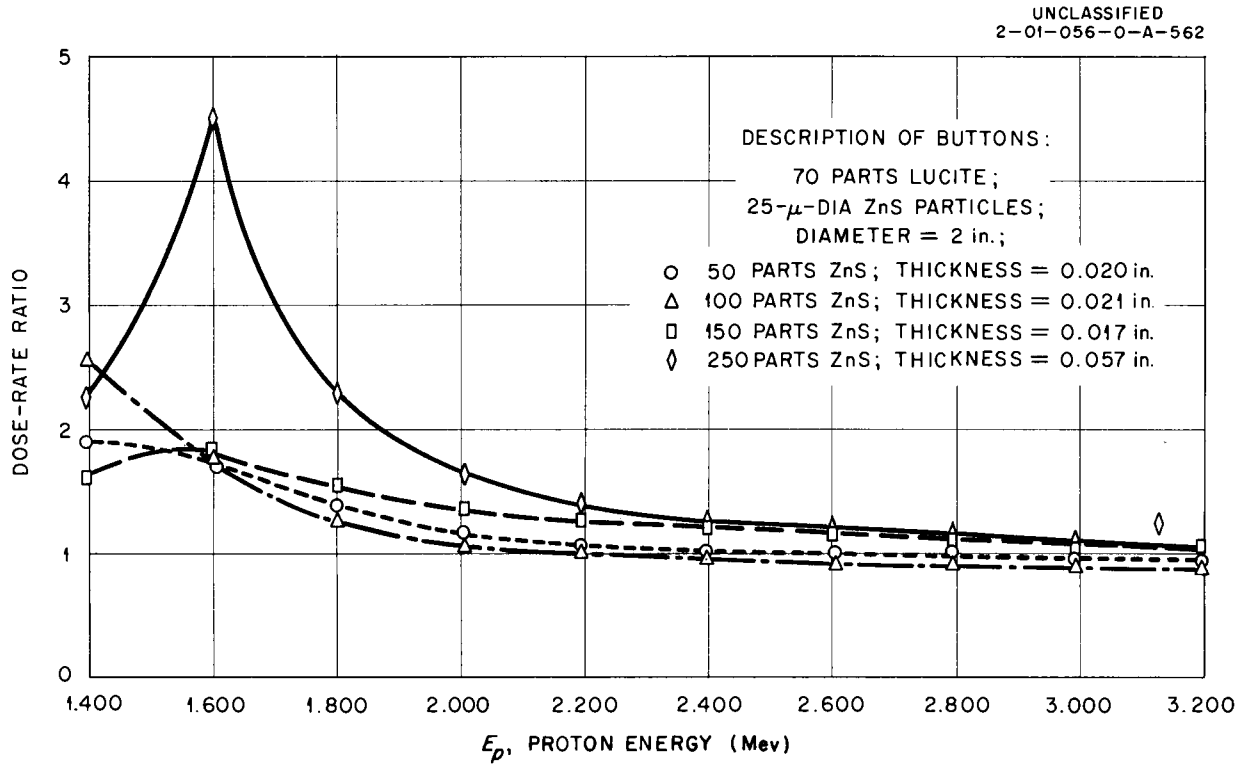

Fig. 6.2.17. Ratio of the Dose-Rate Response of the Dosimeter to the Response of Various Hornyak Buttons to Neutrons from the (p,t) Reaction (Van de Graaff Generator).

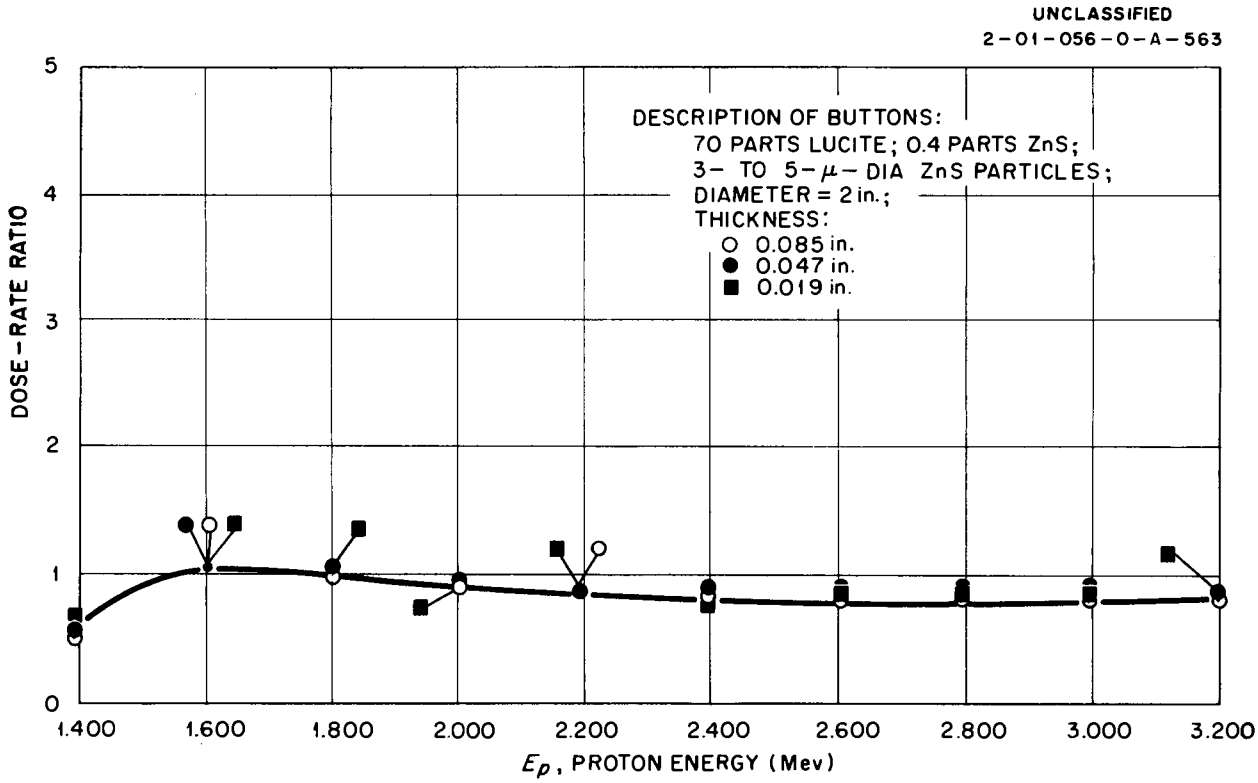

Fig. 6.2.18. Ratio of the Dose-Rate Response of the Dosimeter to the Response of Various Hornyak Buttons to Neutrons from the (p,t) Reaction (Van de Graaff Generator).

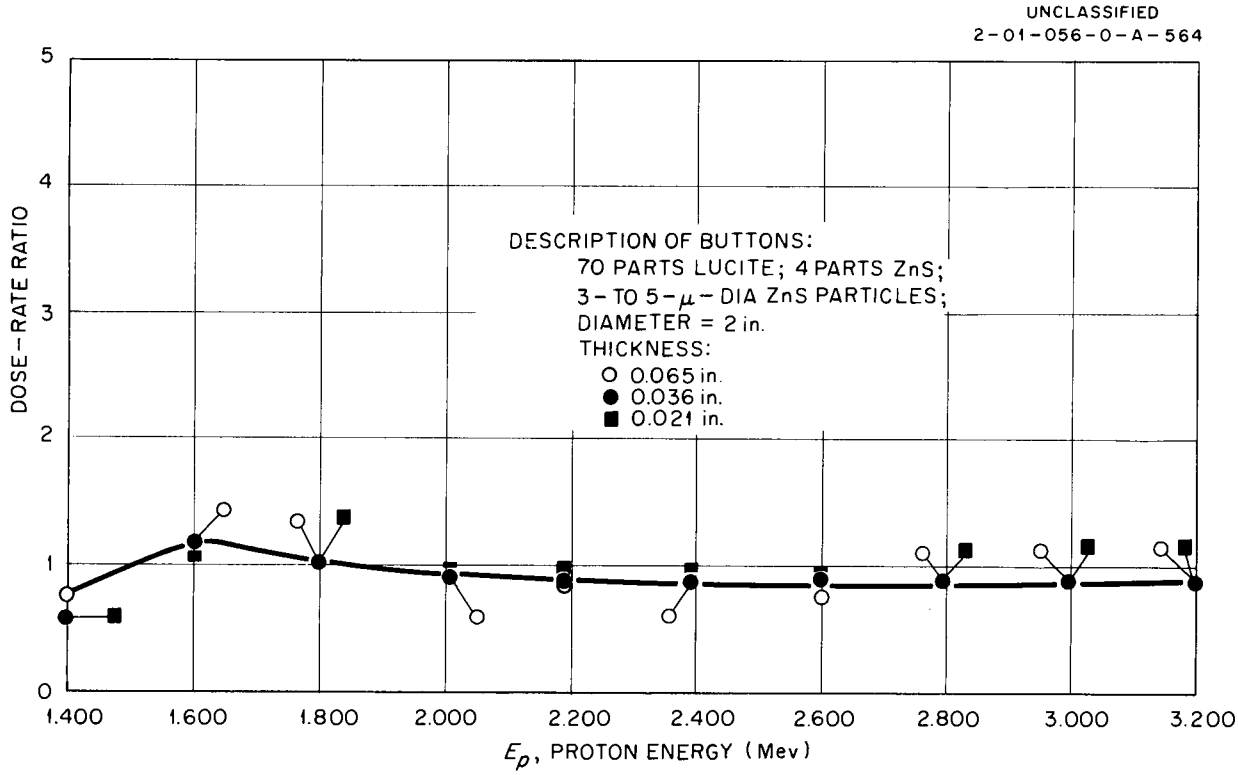

Fig. 6.2.19. Ratio of the Dose-Rate Response of the Dosimeter to the Response of Various Hornyak Buttons to Neutrons from the (p,t) Reaction (Van de Graaff Generator).

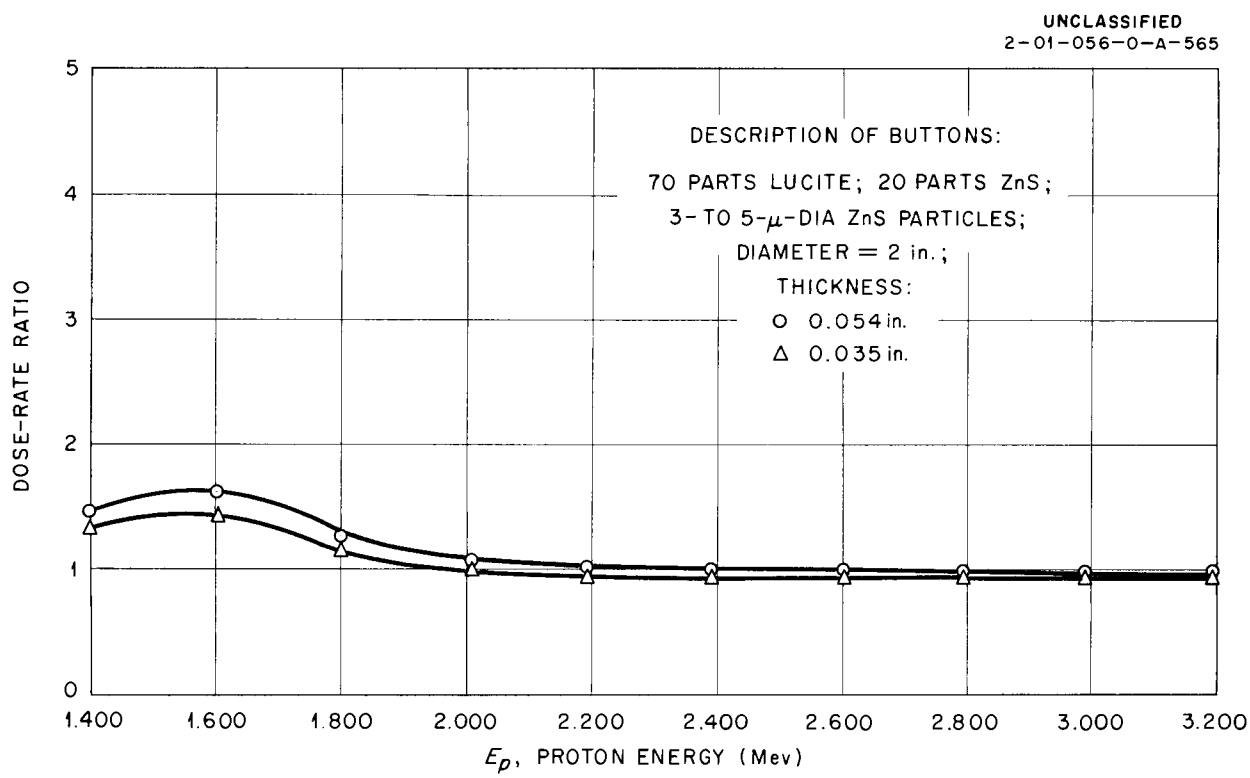

Fig. 6.2.20. Ratio of the Dose-Rate Response of the Dosimeter to the Response of Various Hornyak Buttons to Neutrons from the (p,t) Reaction (Van de Graaff Generator).

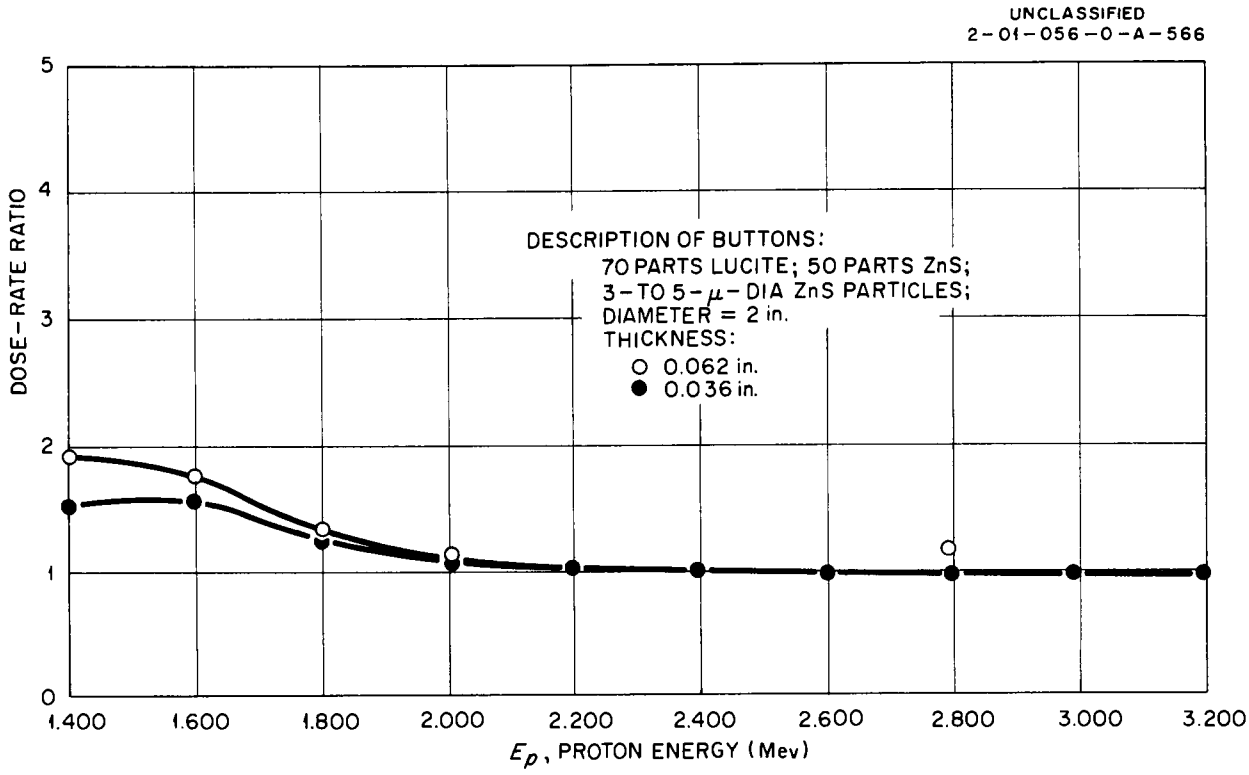

Fig. 6.2.21. Ratio of the Dose-Rate Response of the Dosimeter to the Response of Various Hornyak Buttons to Neutrons from the (p,t) Reaction (Van de Graaff Generator).

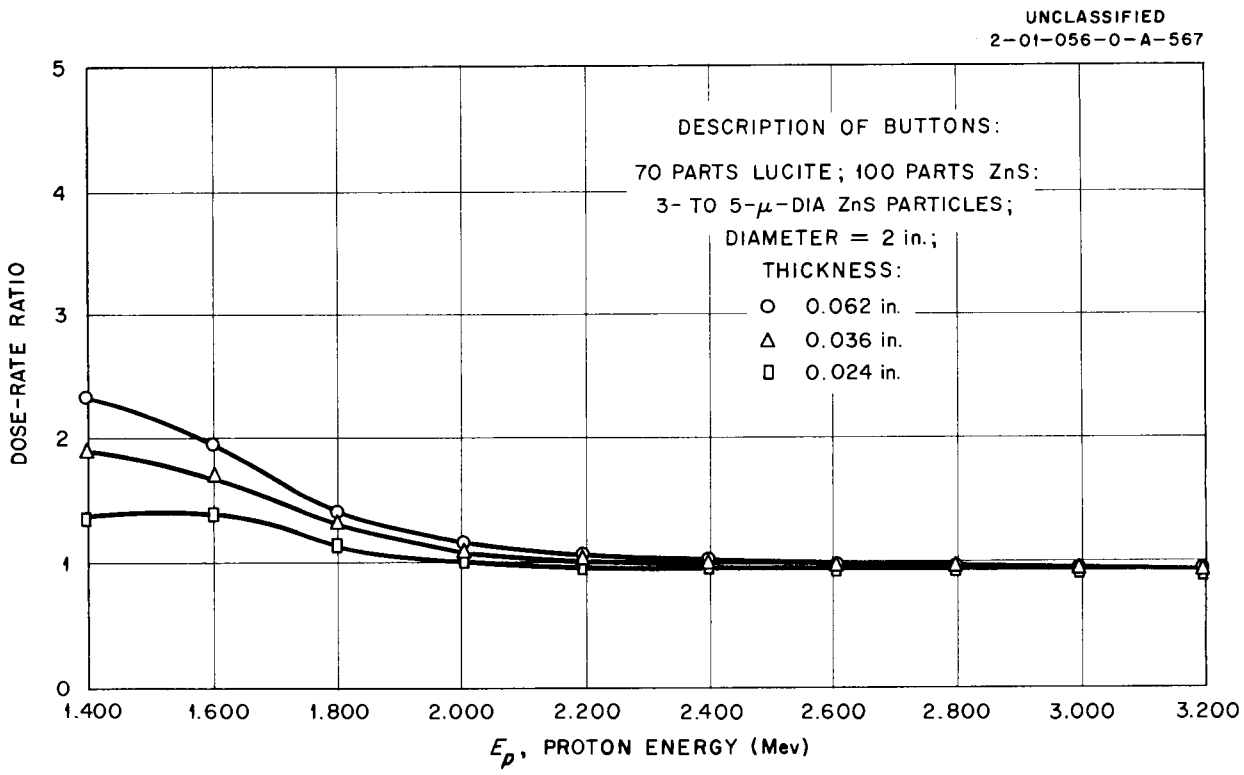

Fig. 6.2.22. Ratio of the Dose-Rate Response of the Dosimeter to the Response of Various Hornyak Buttons to Neutrons from the (p,t) Reaction (Van de Graaff Generator).

rate readings than the dosimeter does for the particular spectra checked.

In the past, neutron dose-rate measurements were made with the dosimeter biased for gamma-ray fields greater than the normal 2 r/hr. In order to take such data, the bias levels on the integrator were changed. For example, to make measurements in a 20-r/hr gamma-ray field the 6- and 10-v bias levels were set at 14 v. It was not known at that time how much difference this made in the measured dose, since the spectrum being measured may have varied considerably. In order to indicate the error that might be encountered, a check has been made with monoenergetic neutrons. For this comparison, the dosimeter was first biased for a 2-r/hr field and compared with the Hornyak button also biased for a 2-r/hr field. The neutron energy was varied between 0.2 and 4.4 Mev. The 6- and 10-v bias levels on the integrator were then set for 14 v to give a total of four levels at that bias. The dosimeter was again calibrated with a Po-Be source and the measurements were repeated. The ratio of the two dose rates is plotted in Fig. 6.2.24. For the lowest neutron energies the ratio of the dosimeter response is nearly 10. The two dose rates agree at about 1.5 Mev. The difference between the actual dose rate at 2 r/hr and that measured with a change in bias levels for 20 r/hr thus depends upon the hardness of the neutron spectrum involved.

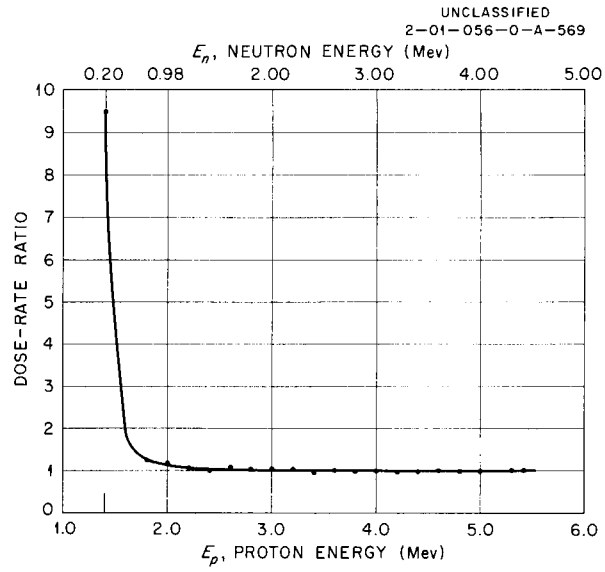

Fig. 6.2.24. Ratio of the Response of the Hurst Type of Dosimeter to 0.2- to 4.4-Mev Neutrons in 2- and 20-r/hr Gamma-Ray Fields.

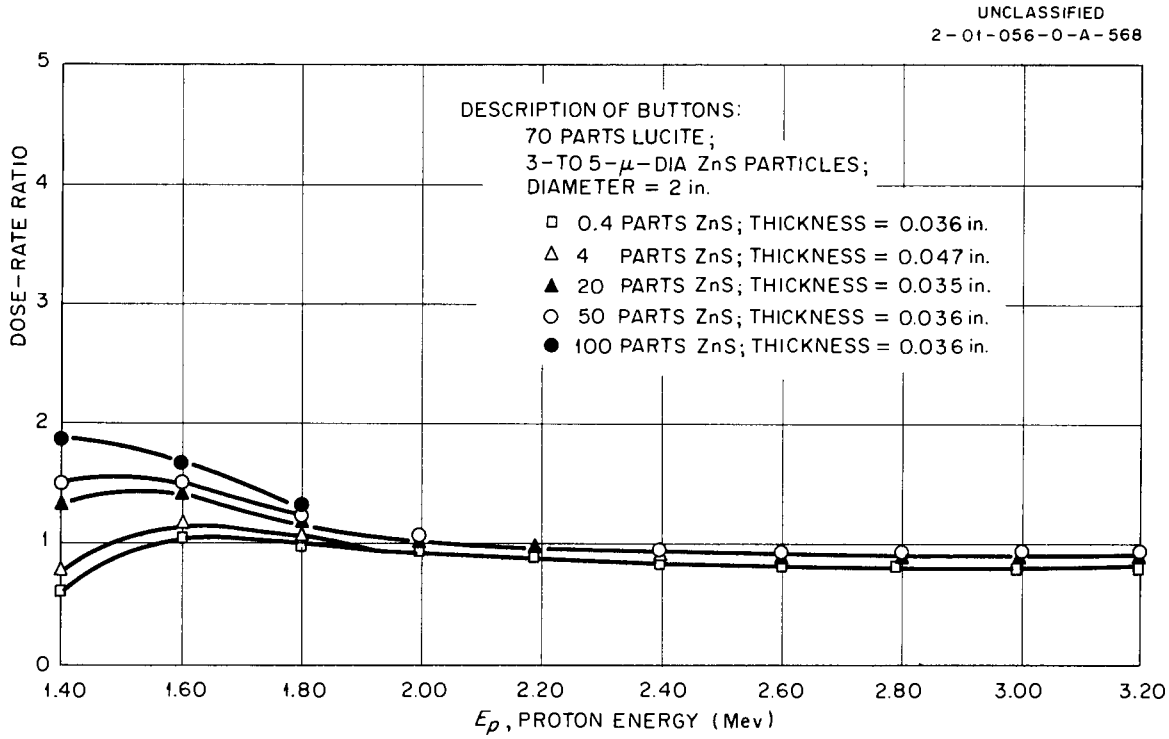

Fig. 6.2.23. Ratio of the Dose-Rate Response of the Dosimeter to the Response of Various Hornyak Buttons to Neutrons from the (p,t) Reaction (Van de Graaff Generator).

6.3. AIRCRAFT SHIELD DESIGN

C. E. Clifford F. L. Keller

MONTE CARLO CALCULATIONS OF FLUXES AND DOSE RATES RESULTING FROM NEUTRONS MULTIPLY SCATTERED IN AIR

J. Hilgeman[1] F. L. Keller
C. D. Zerby

The design of the crew-compartment shield of a nuclear-powered aircraft depends rather critically on the magnitude, angular distribution, and energy spectrum of the radiation which is incident on the exterior surfaces of the crew shield. In order to obtain extensive information concerning these quantities for neutrons which arrive at the crew compartment after scattering in air, the previously developed line-beam Monte Carlo neutron air-scattering code[2] has been utilized. Oxygen and nitrogen cross-section data published in BNL-325[3] are used in this code, and the scattering is considered to be isotropic in the center-of-mass system. The code starts with a line beam of neutrons of initial energy, E_0, which leave the source point at a polar angle θ_0 with respect to the source-detector axis and calculates the flux and dose rate at an isotropic detector located at a specified distance g from the source. The flux and dose rate at the detector are further broken down with respect to the angle of arrival and the energy spectrum of the incoming neutrons.

Calculations were performed for neutrons with initial energies of 0.55, 1.2, 2, 3, and 5 Mev; angles of emission of 2, 15, 30, 60, 90, 135, and 180 deg; and separation distances of 5, 10, 20, 40, 64, and 100 ft. The results of these calculations will be presented in graphical form in a topical report.[4] In all the calculations the density of air was taken to be that at an altitude of 1100 ft above sea level; however, the results may easily be extended to other altitudes and separation distances by making use of appropriate altitude transformations.[5]

The results of these calculations show that the total air-scattered flux, ϕ, at a detector placed a distance g from a line-beam source of 1 neutron/sec of initial energy E_0 leaving the source at an angle θ_0 may be represented by the relation

$$\phi = \frac{\Sigma_s(E_0)}{4\pi g} \frac{\pi - \theta_0}{\sin \theta_0} ,$$

where $\Sigma_s(E_0)$ is the macroscopic scattering cross section of air at the initial energy, E_0. This is the same relation that is obtained from an analytical calculation of the single-scattered flux from a line-beam source under the assumption that the scattering is isotropic in the laboratory system and there is no material attenuation. It was also found that the total air-scattered dose rate, D, at the detector may be represented by

$$D = \frac{C(E_0)}{1.2} \frac{\Sigma_s(E_0)}{4\pi g} \frac{\pi - \theta_0}{\sin \theta_0} ,$$

where $C(E_0)$ is the flux-to-dose rate conversion factor at the initial energy, E_0. Of course, the angular distribution and energy spectra of the neutrons which arrive at the detector differ considerably from the results obtained from single-scattering calculations which assume isotropic scattering in the laboratory system and neglect attenuation and energy degradation. The discrepancy naturally increases with increasing θ_0. Representative plots of angular distributions and energy spectra at the detector will be included in a topical report.[4]

CALCULATION OF AIR-SCATTERED NEUTRON DOSE RATES AROUND A CYLINDRICALLY SYMMETRIC SOURCE

C. A. Goetz[6]

A code has been written for the Oracle with which the neutron dose rate around a cylindrically symmetric source can be calculated. The detector

[1] On assignment from U.S. Air Force.

[2] C. D. Zerby, *ANP Prog. Rep. for Period Ending Dec. 31, 1956*, ORNL-2221, Part 6, p 3.

[3] D. J. Hughes and J. A. Harvey, *Neutron Cross Sections*, BNL-325 (July 1, 1955).

[4] J. Hilgeman, F. L. Keller, and C. D. Zerby, *Monte Carlo Calculations of Fluxes and Dose Rates Resulting from Neutrons Multiply Scattered in Air*, ORNL-2375 (to be published).

[5] C. D. Zerby, *Radiation Flux Transformation as a Function of Density of an Infinite Medium with Anisotropic Point Sources*, ORNL-2100 (Oct. 22, 1956).

[6] On assignment from Pratt & Whitney Aircraft Co.

is located a distance g from the source and at an angle ψ with respect to the axis of symmetry of the source distribution. The geometry for the calculation is illustrated in Fig. 6.3.1. In this figure, α is the angle between a particular neutron direction, $\vec{\Omega}$, and the axis of symmetry of the source; θ_0 is the angle between $\vec{\Omega}$ and the source-detector axis; and ψ is the angle between the axis of symmetry of the source and the source-detector axis. The angle ϕ is the azimuthal angle between the axis of symmetry of the source and $\vec{\Omega}$, as measured from the source-detector axis.

UNCLASSIFIED
2-01-060-24

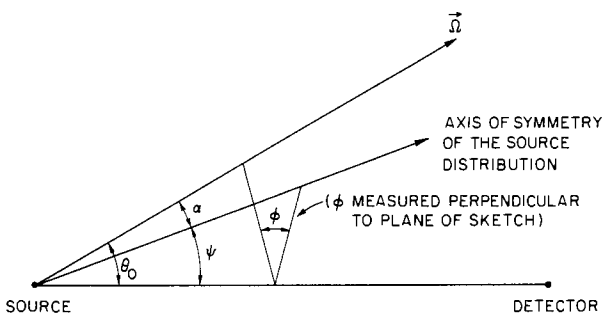

Fig. 6.3.1. Geometry for Calculation of Air-Scattered Neutron Dose Rates Around a Cylindrically Symmetric Source.

The results of the Monte Carlo air-scattering calculation discussed in the preceding paper are used in this calculation. The Monte Carlo calculation supplies a quantity which gives the air-scattered neutron dose rate at a detector located a distance g from a source of neutrons, of initial energy E_0, which leave in a line beam, at an angle θ_0, with respect to the source-detector axis, normalized to 1 neutron/sec in the beam. This quantity, which may be denoted as $P(g,E_0,\theta_0)$, was shown in the preceding section to be represented by

$$P(g,E_0,\theta_0) = \frac{A(E_0)}{g} \frac{\pi_0 - \theta_0}{\sin\theta_0} ,$$

where

$$A(E_0) = \frac{C(E_0)\,\Sigma_s(E_0)}{4.8\pi} ,$$

and

$\Sigma_s(E_0)$ = macroscopic scattering cross section of air at the initial energy, E_0, cm^{-1},

$C(E_0)$ = neutron flux-to-dose conversion factor at the initial energy, E_0, (mr/hr)/(neutron/cm^2·sec).

Hence, if the energy spectrum of the neutrons which leave the source is not strongly dependent upon the angle α, the following average may be defined:

$$\bar{A} = \frac{\int A(E_0)\,N(E_0)\,dE_0}{\int N(E_0)\,dE_0} ,$$

where $N(E_0)$ is the energy distribution of the source neutrons. Actually, $A(E_0)$ is fairly consistent for fast neutrons, and therefore the value of $\bar{A}$ is not extremely sensitive to the shape of $N(E_0)$.

If a source strength, $S(\alpha)$, is defined such that $S(\alpha)\,d\Omega$ is the number of neutrons per second which leave in the element of solid angle $d\Omega$ about $\vec{\Omega}$, the air-scattered neutron dose rate at the detector, $D(\psi,g)$, may be expressed as:

$$D(\psi,g) = \int_{\theta=0}^{\pi} \int_{\phi=0}^{2\pi} S(\alpha)\,\bar{P}(g,\theta_0)\sin\theta_0\,d\theta_0\,d\phi ,$$

where

$$\bar{P}(g,\theta_0) = \frac{\bar{A}}{g} \frac{\pi - \theta_0}{\sin\theta_0} ,$$

and

$$\cos\alpha = \cos\theta\cos\psi + \sin\theta\sin\psi\cos\phi .$$

Thus,

$$D(\psi,g) = \frac{\bar{A}}{g} \int_{\theta=0}^{\pi} (\pi - \theta_0) \int_{\phi=0}^{2\pi} S[\alpha(\theta,\psi,\phi)]\,d\phi\,d\theta .$$

The source strength, $S(\alpha)$, is entered into the machine in tabular form and the machine then carries out the double integration for any specified value of ψ.

This code should be useful in attempts to correlate the results of the Monte Carlo air-scattering calculations with the shapes of air-scattering probabilities as determined from the "broad-beam" experiments at the TSF.